Manuscript Details

Manuscript number	GLOPLACHA_2019_43_R1
Title	A 2000 year record of palaeofloods in a volcanically-reset catchment: Whanganui River, New Zealand.
Short title	2000 year record of palaeofloods: Whanganui River, New Zealand.
Article type	Research paper

Abstract

Palaeofloods in the Whanganui River, North Island, New Zealand are investigated using floodplain sedimentary archives at two locations in the lower Whanganui catchment. The ca. AD 232 Taupo volcanic eruption transformed the lower valley of the Whanganui River, emplacing a substantial volume of volcanogenic mass flow material and providing a new starting point for subsequent alluvial sedimentation. At Atene a high–resolution archive of flood sediments is preserved in a valley meander cutoff in the lower reaches of the Whanganui Gorge, where a ~9 m core was extracted. At Crowley House further down valley, two ~5 m cores were also extracted from a terrace-confined floodplain. Organic material from these cores allows the timing of floods at these sites to be constrained using 11 radiocarbon dates (ten from Atene, one from Crowley House). Flood magnitudes are reconstructed using XRF core-scanned geochemistry as a proxy for flood unit grain size. An age-depth model at Atene identifies three distinct phases of sedimentation with above average flood activity recorded at 1450-1125, 950, 650-500, and 400-325 cal. yr BP, which can be linked to the El Niño Southern Oscillation (ENSO) and strengthening of the Southern Hemisphere Westerly Wind circulation. Large floods also cluster in the late 1800s, reflecting a combination of enhanced storminess and land cover change, which also resulted in deeper erosion of regolith in the catchment, revealed by cosmogenic analysis at Crowley House. Climatic and non-climatic drivers are responsible for floods in the Whanganui catchment over the past ~2000 years, with the largest floods occurring during La Niña and positive Southern Annular Mode conditions. The timing of the largest single flood in the Whanganui in this period is consistent with the volcanic-resetting event itself of AD 232. This study demonstrates the close relationship between regional climate variability in the south-western Pacific Ocean and the occurrence of extreme floods in New Zealand, and the importance of using multi-centennial length hydrological series for effective flood risk assessment.

Keywords	New Zealand floodplain sedimentary archives; valley meander cutoff; Taupo volcanic eruption; El Niño Southern Oscillation / Southern Annular Mode and extreme floods

Corresponding Author	Ian Fuller
Corresponding Author's Institution	Massey University
Order of Authors	Ian Fuller, Mark Macklin, Willem Toonen, Jonathan Turner, Kevin Norton

Suggested reviewers	Tess Harden, Thomas Pierson, Gerardo Benito

Highlights

- New ~2000 yr palaeoflood archive from New Zealand, in the Whanganui catchment, North Island, extracted from abandoned valley cutoff, floodplain and late Holocene terrace.
- Flood series reconstructed using XRF geochemistry as a grain size proxy to identify flood units, combined with a radiocarbon-based age-depth model derived from ten ^{14}C ages in a ~9 m sediment core.
- Archive includes evidence for an extraordinary flood contemporaneous with the ca. AD 232 (1718 ± 5 cal. yrs BP) Taupo eruption.
- Periods of flood activity at 1450-1125, 950, 650-500, and 400-325 cal. yr BP align with hydroclimate proxy evidence for enhanced storminess and river activity elsewhere in New Zealand.
- ENSO variability is identified as the principal control on flood activity in the Whanganui in the last ~2000 yr, albeit within a context of considerable climate complexity.

A 2000 year record of palaeofloods in a volcanically-reset catchment: Whanganui River, New Zealand.

Ian C. Fuller[1], Mark G. Macklin[1,2,3], Willem H.J. Toonen[4], Jonathan Turner[5], Kevin Norton[6]

[1]*Innovative River Solutions & Geosciences Group, School of Agriculture and Environment, Massey University, Palmerston North, New Zealand.*

[2]*School of Geography & Lincoln Centre for Water and Planetary Health, University of Lincoln, Lincoln, UK.*

[3]*Center for the Inland, La Trobe University, Melbourne, Australia*

[4]*Egyptology Unit, Faculty of Arts, Katholieke Universiteit Leuven, Leuven, Belgium.*

[5]*School of Geography, University College Dublin, Dublin, Ireland.*

[6]*School of Geography & Earth Sciences, Victoria University of Wellington, Wellington, New Zealand.*

Abstract

Palaeofloods in the Whanganui River, North Island, New Zealand are investigated using floodplain sedimentary archives at two locations in the lower Whanganui catchment. The ca. AD 232 Taupo volcanic eruption transformed the lower valley of the Whanganui River, emplacing a substantial volume of volcanogenic mass flow material and providing a new starting point for subsequent alluvial sedimentation. At Atene a high–resolution archive of flood sediments is preserved in a valley meander cutoff in the lower reaches of the Whanganui Gorge, where a ~9 m core was extracted. At Crowley House further down valley, two ~5 m cores were also extracted from a terrace-confined floodplain. Organic material from these cores allows the timing of floods at these sites to be constrained using 11 radiocarbon dates (ten from Atene, one from Crowley House). Flood magnitudes are reconstructed using XRF core-scanned geochemistry as a proxy for flood unit grain size. An age-depth model at Atene identifies three distinct phases of sedimentation with above average flood activity recorded at 1450-1125, 950, 650-500, and 400-325 cal. yr BP, which can be linked to the El Niño Southern Oscillation (ENSO) and strengthening of the Southern Hemisphere Westerly Wind circulation. Large floods also cluster in the late 1800s, reflecting a combination of enhanced storminess and land cover change, which also resulted in deeper erosion of regolith in the catchment, revealed by cosmogenic analysis at Crowley House. Climatic and non-climatic drivers are

responsible for floods in the Whanganui catchment over the past ~2000 years, with the largest floods occurring during La Niña and positive Southern Annular Mode conditions. The timing of the largest single flood in the Whanganui in this period is consistent with the volcanic-resetting event itself of AD 232. This study demonstrates the close relationship between regional climate variability in the south-western Pacific Ocean and the occurrence of extreme floods in New Zealand, and the importance of using multi-centennial length hydrological series for effective flood risk assessment.

Keywords

New Zealand floodplain sedimentary archives; valley meander cutoff; Taupo volcanic eruption; El Niño Southern Oscillation / Southern Annular Mode and extreme floods.

1. Introduction

High resolution multi-centennial and millennial flood records have been successfully reconstructed from alluvial archives (Jones *et al.*, 2012, Toonen *et al.*, 2015; Fuller *et al.*, 2018). Palaeoflood data can be incorporated into flood-frequency analysis (Longfield *et al.*, 2018) and allows extension of flood series. This improves flood-risk assessment as gauged flood records are generally short, rarely exceeding a century (Wilhelm *et al.*, 2018a). In New Zealand at the turn of the 21st century, gauged records rarely exceed 50 years (McKerchar and Henderson, 2003). The probability of gauged records capturing low frequency, high magnitude floods is therefore low, which in turn limits our understanding of their causes (Wilhelm *et al.*, 2018b). Yet it is these rare-low frequency flood events that pose the greatest risk to human life and infrastructure, because society is under-prepared for them (see Dettinger, 2011).

The occurrence of floods exhibits marked variability over time in response to changing synoptic and atmospheric circulation regimes (McKerchar and Henderson, 2003; Dettinger, 2011; Macklin *et al.* 2012), including the El Niño Southern Oscillation (ENSO), e.g. Ely *et al.* (1993), Kiem *et al.* (2003), Ward *et al.* (2014), Munoz and Dee (2017); and North Atlantic Oscillation (NAO), e.g. Macklin and Rumsby (2007), Wilhelm *et al.* (2012), Schulte *et al.* (2015), Foulds and Macklin (2016). Predicted climate warming is likely to change future flood magnitude and frequency as the hydrological cycle intensifies (Knox, 2000, Hirabayashi *et al.*, 2013; Kundzewicz *et al.*, 2014; Blöschl *et al.*, 2017). Hence, there is a need to better understand relationships between climate and flooding in light of the changing timing, magnitude and frequency of floods (Wilhelm *et al.*, 2018a). This understanding requires longer flood series, which can be compared with other hydroclimatic records, and in turn used to identify underlying climatic and anthropogenic forcing (Toonen et al. 2017; Munoz *et al.*, 2018).

In comparison with middle latitude regions of the Northern Hemisphere, we understand less of regional climate controls of flooding in the temperate latitudes of the Southern Hemisphere. Particularly complex are the hydroclimatic teleconnections between ENSO and the Southern Annular Mode (SAM) (also known as the Antarctic Oscillation) that drive the strength and trajectories of the Southern Hemisphere Westerly Winds (SHWW) (Xia *et al.*, 2018). The location and strength of the SHWW is critical for moisture delivery from the Southern Ocean to temperate land masses in the Southern Hemisphere (Moreno *et al.*, 2018), and is therefore likely to play a key role in flood magnitude and frequency variability. Richardson *et al.* (2013) concluded from a national-scale meta-analysis of more than 400 ^{14}C dated flood units that centennial-scale variability in Holocene river activity in New Zealand was driven by a combination of SAM-like and ENSO-like synoptic patterns,

with stronger SHWW in a more zonal circulation attributed to El Niño- and negative SAM-like conditions favouring enhanced river activity in the South Island. In contrast, weakening of the SHWW and a more meridional circulation attributed to La Niña- and positive SAM-like conditions appeared to enhance North Island river activity. Although Richardson *et al.* (2013) where able to identify multi-centennial length flood rich and poor phases in both North and South Island, they were not able to assign estimates of flood magnitude to individual events. Nevertheless, Ummenhofer and England (2007) have demonstrated that variability in precipitation across New Zealand is modulated by ENSO and SAM at an interannual timescale and these climate modes are therefore likely to drive not only large-scale river activity, but also discrete episodes of extreme flooding.

To better understand the relationship between flooding and short and long term climate change in New Zealand requires both a long as well as high resolution record of extreme hydrological events. Our recent work in the Manawatu catchment showed promise in this regard, reporting a ~3000-year record of flooding from a series of infilled palaeochannels in the lower Manawatu floodplain (Fuller *et al.*, 2018). However, linking that flood archive with climate proxy records proved difficult because of limited dating control. In this paper we turn our attention to the Whanganui River, located ~50 km to the northwest of the Manawatu (Figure 1a) in an effort to recover an event scale record of flooding over the last 2000 years.

2. Regional setting

2.1 Catchment characteristics

The 7380 km^2 Whanganui River catchment offers potential for the formation and preservation of high resolution palaeoflood archives because its geology is largely weakly lithified sandstone, siltstone and mudstone of the Wanganui Basin, a major structural depression that accumulated up to 4000 m of marine sediment above the greywacke basement during the Plio-Pleistocene (Soons and Selby, 1992). River entrenchment of these soft mudstone lithologies in response to Late Quaternary uplift rates of around 0.3 - 0.6 m ka^{-1} (Pillans, 1990) in the lower and middle catchment has produced a narrow confined valley and gorge (cf. Figure 1). Large, deep-seated slope failures are common in similar mudstone terrain in the North Island (cf. Dellow *et al.*, 2005; Massey *et al.*, 2013; McColl and McCabe 2016) and over 100 deep-seated prehistoric landslides have been mapped in south-eastern Taranaki, which includes the western Whanganui catchment (Crozier and Pillans,

1991). The Whanganui catchment is also prone to large earthquakes, with the largest since European colonisation estimated at M_w 7.5 in July 1843 (Eiby, 1968). This earthquake, together with an earlier M_w 6-7 in 1838 produced an unquantified number of very large landslides in the Whanganui catchment (Crozier and Pillans, 1991). The combination of narrow valleys, landslide-prone terrain and earthquakes brings with it the potential for landslide damming of the main river and its tributaries (Watson, pers. comm. 2017). Erosion of soft-rock hill country generates high suspended sediment loads, the modern suspended sediment yield of the Whanganui River is 4.7 Mt yr-1 (Hicks *et al*., 2011). Gravels in the river are derived from more indurated volcanics in the north-east of the catchment where the river drains the central plateau of the Taupo Volcanic Zone. Located in the eastern headwaters of the catchment is Mt. Ruapehu (cf. Figure 1), which has a crater lake at its summit from which (historically small) lahars have been generated and fed into the Whanganui during eruption episodes. Tost and Cronin (2016) highlight that much larger scale volcanic mass flows from Ruapehu edifice collapse have inundated the upper Whanganui during the Late Pleistocene.

Figure 1

The Taupo eruption, ca. AD 232 ± 5 (AD 224-240 2σ calendar date range, 1718 ± 5 cal. yr BP) (Hogg *et al*., 2012), emplaced ignimbrite in the eastern Whanganui River basin, impacting ca. 43% of the catchment (cf. Figure 1b) (Manville *et al*., 2009). This material was rapidly reworked by runoff and channelised flow and deposited in the lower Whanganui valley forming the 'Taupo Pumice Alluvium' that underlies late Holocene and historical fluvial deposits in the region (Manville *et al*., 2009). The emplacement of mass flow deposits immediately following the Taupo eruption reset the lower Whanganui valley floor by obliterating older alluvial deposits and landforms so the flood sedimentary archive only covers the last 1800 years.

2.2 Whanganui flood records

Gauged since 1957 at Te Rewa (Figure 1b, catchment area 6643 km^2), the mean flow of the Whanganui River is 221 m^3s^{-1}, and the mean annual flood calculated at 2230 m^3s^{-1}, with a coefficient of variation (measure of flow variability by dividing standard deviation of instantaneous flows by mean flow) of 1.2 (Manville *et al*., 2009). In June 2015 the largest recorded flood in the ~60 year record to date in the Whanganui River was gauged at Te Rewa (Figure 1b), measuring 4755 m^3s^{-1}.

The June flood event was estimated to have an annual return period of 85 years based on a flood frequency analysis of the 59 annual maxima from 1957 to 2015 (inclusive), with a censored assessment including 12 historical peaks dating back to 1858 (Blackwood & Bell, 2016) (cf. Figure 2). The three earliest floods documented in this series have all been assigned the same value; these are estimated flood volumes based on flood height in Whanganui City, which is subject to tidal ponding.

Figure 2

2.3 Climate drivers of flooding

Multiple climate drivers are responsible for contemporary and historical episodes of flooding in New Zealand and these vary on a seasonal, annual and decadal basis. Griffiths (2011) has discussed the role of ENSO, SAM and the Indian Ocean Dipole (IOD) in affecting extreme daily rainfalls and flood generation in New Zealand. During El Niño, enhanced westerly winds tend to increase summertime precipitation in the west especially; during La Niña more northeasterly winds occur, increasing rainfall across New Zealand especially in winter; positive SAM brings wetter conditions to the north and east North Island, negative SAM conversely induces wetness in the south and west; a positive Indian Ocean Dipole weakens storm-tracks reducing precipitation across New Zealand (Griffiths, 2011). Jiang *et al*. (2013) assessed the interactions between ENSO, SAM and the Interdecadal Pacific Oscillation (IPO). IPO operates in positive and negative phases, with positive phases associated with strengthened westerly circulation. Jiang *et al*. (2013) concluded that ENSO, SAM and IPO influence New Zealand climate by modulating the frequencies and intensity of synoptic systems, and argue that in this regard ENSO and SAM appear to be more significant than IPO. In the Whanganui River catchment, Qiao (2012) found that rainfall and streamflow reduced in 1981 and 1998 during intense El Niños, but an increased frequency of high rainfall events in 1988 and 1994/1995 occurred during pronounced La Niña events. The relationship between river flow and SAM has more recently been explored by Li and McGregor (2017), finding an association between enhanced river flows in central and western North Island catchments (including Waikato and Whanganui) with negative SAM, during which the Whanganui catchment receives anomalously strong air flow from the west and associated moisture advection. This effect was observed most clearly in winter.

3. Methods

To investigate the palaeoflood history of the lower Whanganui River, sediment cores were retrieved at three locations using percussion coring. Two ~5 m cores were collected from the infill of abandoned channels at Crowley House. Crowley House 1 was collected from a palaeochannel within the present floodplain, Crowley House 2 was collected from a late Holocene terrace, 1 m above the floodplain (Figure 1d,h). The ~9 m Atene core was collected from the infill of a valley meander cutoff in the lower Whanganui Valley (Figure 1e,g). Core segments of 1 m were transferred to Massey University, where they were split along their vertical axis and their sedimentary characteristics logged. One half of the Crowley House cores was sent to Aberystwyth University (United Kingdom) for geochemical analysis and grain-size laser diffraction analysis. One half of the Atene cores was sent to University College Dublin (Ireland) for high-resolution geochemical analysis. Samples for ^{14}C dating were collected from the core halves that remained at Massey University.

3.1 X-ray Fluorescence geochemistry

A portable Niton GOLDD XRF was used to collect elemental data from the Crowley House cores. In the upper 30 cm of cores a fixed 2 cm measurement interval was used to identify concentrations of anthropogenic (contaminant metal) pollutants. Below that level, a 5 cm sample interval was used down to the bottom of the cores at 5 m. The device was set-up to measure element concentrations (in ppm) for a measurement time of 60 s. The combination of element concentrations and laser diffraction grain-size information (section 3.2) was used to establish a correlation between bulk geochemistry and sediment grain size for the lower reaches of the Whanganui catchment.

On the Atene core, an XRF Itrax core scanner was used to acquire geochemical data. Element counts were established using a 30 s measurement time and a 500 µm sample interval was used to produce a high-resolution record of palaeoflood events (see section 3.4). Invalid measurements (resulting from cracks and small voids in the cores) and low readings (less than 10,000 counts per second) were filtered and removed from the data set. Raw counts are affected by variations in water and organic content, so all measurements were normalised to produce a homogeneous record that reflects variations in bulk sediment grain sizes (Jones *et al*., 2012).

3.2 Grain-size measurements

A Malvern laser diffraction particle sizer was used to measure the grain-size distribution of sediment samples from the Crowley House cores. A refraction index of 1.7 was used, and a particle absorption

index of 0.01, based on the siliciclastic geology of the region. A total of 101 samples was collected from both Crowley House sites: on average every 10 cm. Sample positions respected stratigraphic units ensuring that samples were equally distributed over the full range of textures present in the cores. Demineralised water was added to the samples to create a suspension, which was put in an ultrasonic cleaner device to disperse grains. 300 mg of sodium-pyrophosphate was added to the samples to prevent flocculation. Volumetric contributions were measured in 24 predefined grain-size classes, in the range between 0.5 and 2000 µm.

3.3 Dating and age-depth modelling

Ten samples containing organic macrofossils were collected from various levels in the Atene core. One sample of organic material was recovered from near the base of the Crowley House 1 core. All samples were sent for AMS ^{14}C dating at the Radiocarbon Dating Laboratory of the University of Waikato. Nine of the Atene samples produced a stratigraphically consistent ^{14}C date (Table 1); calendar dates were calculated using the SHCal13 atmospheric calibration curve (Hogg *et al*., 2013). An Oxcal U-Sequence linear deposition model was used to create an age-depth model (Bronk Ramsey, 2009). At the depths of 175 cm and 596 cm, levels for change boundaries were added to the model, corresponding with changes in lithology (section 4.1). Present ground level was prescribed an arbitrary age of 0 ± 50 cal. yrs BP, based on the assumption that these are tributary stream deposits from roughly the last century. No recent floods, including the June 2015 event, could be used as independent time markers in the age-depth model of the upper part of the core, as gauged floods since 1957 have not inundated the Atene core site (section 4.1.1).

Table 1. Overview of AMS radiocarbon ages

Sample	Lab Code	Site	Depth (cm)	^{14}C date yrs BP (±1σ)	Cal. yrs BP (±2σ)	Material
A1	Wk45259	Atene	215	457 ± 15	460-510	Wood
A2*	Wk47414	Atene	347	1334 ± 16	1180-1270	Peat
A3	Wk47415	Atene	398	1289 ± 16	1080-1270	Peat
A4	Wk47416	Atene	443	1302 ± 18	1160-1270	Peat
A4a	Wk47417	Atene	499	1585 ± 18	1370-1520	Peat

A6a	Wk47418	Atene	528	1721 ± 19	1530-1620	Peat
A7	Wk47419	Atene	596	1789 ± 19	1590-1710	Peat
A9	Wk47420	Atene	699	1839 ± 19	1690-1750	Peat
A10a	Wk47421	Atene	720	1874 ± 16	1710-1830	Peat
A11	Wk45269	Atene	773	1944 ± 15	1820-1900	Wood
Crowley 1**	Wk43330	Crowley House 1	470	1133 ± 20	930-1060	Bark fragments

*stratigraphically inconsistent and identified by the Oxcal bootstrap procedure as a statistical outlier: not used in Atene age-depth model.

**A single sample was reported from Crowley House, being the only organic material recovered from this site.

3.4 Cosmogenic isotope analysis

The Crowley House 1 core was sampled to assess the profile of meteoric ^{10}Be through the sedimentary sequence to understand potential variability in catchment erosion rates (e.g. Willenbring and von Blanckenburg, 2010). In this framework, higher concentrations of meteoric ^{10}Be in the sediment could reflect slower basin-wide erosion rates if beryllium profiles are exponential as suggested by Willenbring and von Blanckenburg (2010). Eleven equally spaced samples were taken from the surface through to the base of the core at 5 m depth. We targeted clay lenses within the core in order to minimize grain-size effects. The samples were sieved to 63-90 µm before extracting the reactive ^{10}Be using sequential leaching (Wittmann *et al*., 2012). Approximately 0.3 mg of ^{9}Be carrier (VUW-PK2, derived from phenacite) was added to each sample. Beryllium was separated using standard methods (Norton *et al*., 2008). The ^{10}Be/^{9}Be ratios were measured relative to SRM4325 with a nominal ratio of $2.79+/-0.03*10^{-11}$ at GNS Science on the 0.5MV XCAMS accelerator. We used an assumed meteoric ^{10}Be flux of $1.1x10^{6}$ atoms/cm^2/yr (Heikkila, 2007) and a sediment bulk density of 1.2 g/cm^3 for our interpretations.

3.5 Palaeoflood magnitude estimates

The relative magnitudes of palaeoflood events of the last two thousand years were based on the combination of flood unit grain size and their recurrence interval over the length of record. Commonly deployed geochemical element ratios (cf. Jones *et al*., 2012; Fuller *et al*., 2018; Wilhelm *et al*., 2018b) were tested on laser diffraction grain-size measurements to identify a reliable geochemical proxy for variations in grain size. At Crowley House, the ratio between Zirconium and Rubidium (Zr/Rb) showed a good correlation with D_{50} grain-size measurements ($r = 0.70$, $p < 0.01$; Figure 3). As all research sites are located in the same region, this element ratio was also adopted to interpret variations in texture at Atene. All Zr/Rb data were detrended using a n=101 sample window to assess changes in the local conditions (background sedimentation) that are not related to main river flood magnitudes; for example, vertical changes in river bed height can directly influence the grain size of overbank deposition by raising (channel aggradation) or lowering (channel incision or entrenchment) flood levels of similar size events. The extent of lateral channel movement at both Crowley House and Atene over the last 1800 years or so has been very limited (probably not exceeding the current channel width of c.120 m, cf. Figure 1d), as the river channel is confined by valley sides and terraced Taupo Pumice Alluvium at these sites (cf. Figure 1d, e). For each stage of channel-infilling (section 4.1), the detrended Zr/Rb values were converted into Z-scores ($\frac{x-\mu}{\sigma}$), providing a relative grain size of each flood unit in comparison to the surrounding matrix. The age-depth model provided the total elapsed time in each sedimentary phase and these periods were divided by the frequency of events exceeding a specific Z-score to derive a recurrence time for each flood (or coarse grained) unit.

Figure 3

4. Results and Interpretation

4.1 Channel-fill facies and depositional phasing

4.1.1 Atene

The channel-fill facies at the Atene site can be divided into three main phases on the basis of depositional style and bulk geochemistry (Figure 4). Lithofacies A between c. 6-9 m, lithofacies B between 1.75-6 m and lithofacies C between 0-1.75 m. Lithofacies A is characterised by organic-rich sandy sediments that were deposited between c. 2.0 and 1.7 ka BP (samples A11 to A7, Table 1). Accumulation rates were high averaging 29 mm/yr. Taking into consideration the uncertainty bands

of the age-depth model, accumulation rates may have been even higher, and deposition of this unit may have occurred in less than a 100 years or perhaps even in a few decades .

Lithofacies B mostly comprises silty clays with intercalated mm-cm thick units of fine sands. This is shown by the bulk geochemistry with a progressive decrease in Zr and Si concentrations, interrupted by sharp increases of these elements within sandy flood units, and relatively high levels of metallic elements (such as Iron (Fe), Copper (Cu), and Nickel (Ni)). Average accumulation rates were ca. 3 mm/yr and this unit was deposited between 1.7-0.25 ka BP (samples A6a to A1, Table 1).

Lithofacies C had higher sedimentation rates than lithofacies B with increased accumulation rates of ca. 7 mm/yr in the last few centuries (0.25-0 ka BP). Lithofacies C is not markedly different in texture from those in lithofacies A. However, increases in Aluminium (Al), Manganese (Mn) and Fe, that could be related to (weak) soil formation in this upper part of the core, and its more massive structure distinguishes it from underlying sediments.

Figure 4

Rapidly deposited coarse-grained sediments are commonly found at the base of channel-fill sequences (Toonen *et al*., 2012). As a meander bend gets cut-off from the active channel that has created a new course, a partly open connection is often maintained, which promotes the diversion of flow and bedload sediments into the abandoned channel. The base of the channel-fill and lower few metres are dated immediately prior to the VEI-7 Hatepe eruption of the Taupo Volcano around 1.7 ka BP (1718 ± 5 cal. yr BP) (Hogg *et al.*, 2012). This suggests that the connection between the Atene valley and the active river was maintained until that event. Sedimentation of Taupo Pumice Alluvium subsequently plugged the ends of the Atene valley meander cutoff, disconnecting it from all but overbank flood flows. Taupo Pumice Alluvium was not present at the base of the Atene core, although it plugs both ends of the valley meander cutoff (Figure 5).

Lithofacies B represents the phase in which the abandoned channel was fully disconnected from active river flow, following plugging of the Atene valley meander cutoff by Taupo Pumice Alluvium. Sedimentation became limited to events that exceeded bankfull levels, reflected by lower sedimentation rates and a reduction in grain size. The increase in sedimentation rates in the upper part of the core (lithofacies C) coincides with European colonisation of New Zealand since the beginning of the nineteenth century that was associated with large-scale deforestation, increased

catchment erosion and accelerated floodplain deposition (Beatson & Whelan, 1993). The bed of the Whanganui River incised during this period, and few, if any, main channel floods inundated the Atene site, including the June 2015 flood event. The geochemistry (increased Al, Mn and Fe) and more massive nature of sediments at the top of this core (Figure 4) indicate a greater contribution of more local sources, including very small tributary streams that flow into margins of the Atene valley meander cutoff. The sedimentary record of lithofacies C probably is best interpreted as a record local precipitation intensities and runoff rather than one of exceptional main river floods. Although, there do appear to have been at least two major floods evident at c. 50 and 20 cm, which are picked out by high Z-scored texture and Zr/Rb ratios. These are likely to relate to large floods recorded in the Whanganui catchment during the second half of the 19th century and first decade of the 20th century, and may represent the last time that the Atene valley meander cutoff was inundated by floods generated by trunk river flow. Although these floods were smaller than June 2015 (cf. Figure 2), trunk river incision in the last ca. 100 years may explain this scenario.

Figure 5.

4.1.2 Crowley House

The Crowley House 1 core (CH1) (Fig. 6) provides a flood record for the last ~1000 years, based on a radiocarbon date at 4.7 m (Table 1). The lower part of the core is relatively sandy, and the upper ca. 2 m fines upwards and grades into clays near the surface. The uppermost decimetre was deposited by the June 2015 flood - the core was collected in February 2016. In addition to the 2015 flood unit at the surface, several flood units can be observed in the lower half of the core with the largest Zr/Rb peak around 4.6 m, which lies 0.1 m above the radiocarbon date of 930-1060 cal. yr BP. Elevated concentrations of lead (Pb) resulting from modern pollution are found only in the upper 50 cm of the core.

^{10}Be concentration in CH1 generally increases towards the surface (Figure 6). Willenbring and von Blanckenburg (2010) showed that meteoric ^{10}Be concentrations in river sediments can be used to calculate basin-wide erosion rates if erosion is steady and ^{10}Be decreases exponentially with depth. Following this interpretation, the increasing ^{10}Be concentrations towards the surface at Crowley House would indicate an overall decrease in surface erosion during the past millennium. This seems unlikely as many authors have shown rapid increases in erosion rates in New Zealand upon human

arrival and land use intensification (e.g. Wilmshurst *et al.*, 1999; Kettner *et al.*, 2007; Richardson *et al.*, 2014; Fuller *et al.*, 2015). As demonstrated by Graly *et al*. (2010), many soil profiles globally display a marked increase in ^{10}Be with depth as meteoric beryllium is concentrated in clay rich soil horizons. Graly *et al*. (2010) also note that this subsurface peak cannot be explained by grain-size effects. If the catchment soils here follow this trend, then a more likely explanation for the ^{10}Be concentrations is that deforestation and agricultural intensification since the beginning of the nineteenth century has resulted in deeper erosion, accessing soil B-horizon material throughout the catchment. This interpretation could also be reflected in the overall reduction in grain-sizes delivered and the lower Zr/Rb ratios. We suggest that the relatively stable ^{10}Be concentrations at depth in CH1 are indicative of the long-term basin-wide erosion rate of ~200-300 mm/kyr. Erosion rates at shallower depths would be faster, but not calculable since a steady state has been violated (Willenbring and von Blanckenburg, 2010).

Crowley House 2 (CH2) is located on a terrace 1 m above the CH1 core site. This terrace was not inundated by flood water in June 2015. The lower part of the core comprises fine sands (Fig. 6), and between 2-3 m depth deposits grade into silts, which extend to the modern surface. No radiometric dating is available for CH2.

Figure 6.

4.2 Palaeoflood and storminess records

Based on the age-depth model of sedimentation at Atene and its normalised Zr/Rb record , the relative magnitudes of flood units were estimated as a recurrence time (Figure 7). The frequency of overbank deposition changed over time in response to changing connectivity between the main channel of the Whanganui River and the Atene valley meander cutoff. During the deposition of lithofacies A, high connectivity and sedimentation rates enables reconstruction of events with a recurrence time of less than a decade. For lithofacies B, only events with a recurrence interval of more than 30 years were recorded. This suggests that the Atene valley meander cutoff was progressively disconnected from the Whanganui River, by both sedimentation in the cutoff and incision of the straightened channel at that time, with overbank sediments reaching this location only during rare high-magnitude events. When further incision and / or sedimentation of the

channel in the last centuries left the Atene site out of reach of Whanganui river floods, the sediment supply in the abandoned loop was primarily sourced from small tributaries that drain into the Atene valley meander cutoff.

At ca. 5.8 m depth in the Atene core, coinciding with the transition of lithofacies A to lithofacies B, the largest by-proxy flood event appears (Figure 7, Table 2). The estimated recurrence time of this event exceeds 35,000 years, which obviously cannot be taken at face value, but does indicate a very rare and anomalous large flood. The age-depth model places this event to around AD 200 (1750 cal. yrs. BP), which is very close to the Taupo eruption of AD 232 (1718 ± 5 cal. yr BP Hogg *et al*., 2012). This indicates that immediately prior to, or even coincident with plugging of the Atene valley meander cutoff, an exceptionally large flood occurred in the lower Whanganui valley that deposited a very coarse flood unit at Atene. This could have been a lahar or may reflect a catastrophic dambreak flood, either of which might explain the anomalous large grain size of these overbank deposits. The rest of lithofacies B shows a series of moderately-sized (multi-decadal) events and several large floods. These floods however were likely larger than the largest recorded flood in the Whanganui, which occurred in June 2015, gauged at 4755 m^3s^{-1} with an 85 year annual recurrence interval (Blackwood and Bell, 2016). The next largest event in lithofacies B at 4.5 m is ranked second in the entire record, has a ca. 915-year recurrence and is dated to ca. AD 650 (1300 cal. yrs BP) (Table 2). Several events of ca. 250-yr recurrence are found at 4.3, 3.4, 3.1, and 1.8 m , with dates of ca. AD 725 (1225 cal. yrs BP), 1025 (925 cal. yrs BP), 1150 (800 cal. yrs BP), and 1600 (350 cal. yrs BP), respectively (Figure 7, Table 2). These events are likely also to be recorded downstream in core CH1 (Figure 6), which records flooding in the lower Whanganui valley over the last thousand years or so. A major flood unit is evident just above the level that was dated to ca. AD 955 (930-1060 cal. yrs BP) (Figure 5), which would be consistent with a large flood event recorded at Atene at ca. AD 1025 (925 cal. yrs BP).

The recurrence interval for local runoff events in lithofacies C is based on relative grain size in the profile. As with estimating the magnitude of floods in lithofacies A and B, it is assumed that the most intense precipitation and runoff contributed the coarsest sediments, with the additional possibility of trunk river inundation. Two major events can be recognised in the upper metre of the Atene core, at depths of 0.2 and 0.5 m (Figure 7). The event at 0.2 m has an associated recurrence time of ca. 70 years and could relate to the last inundation of the cutoff by a flood of slightly smaller magnitude than June 2015 in the late 1800s or very early 1900s prior to disconnection by trunk river incision. At 0.5 m depth the event has an associated recurrence interval of ca. 240 years, so probably reflects either (i) very intense local precipitation and runoff or (ii) a very large flood from the trunk

409 river that inundated the cutoff in the early 1800s (Table 2). Further work at the site is needed to
410 clarify these potential sources.

411

412 **Figure 7.**

413

414 *Table 2. Overview of large (palaeo)flood events, as recorded at Atene.*

415

Age BP (yrs)	**Estimated Date (AD)***	**Depth (m)**	**Recurrence Time (yrs):** (min) **avg** (max)	**Remarks**
50 (±50)	ca. 1900 (past century)	0.2	(50) **70** (90)	Major storm, last inundation?
150 (±50)	ca. 1800 (first half 19th century)	0.5	(170) **240** (320)	Major storm and / or flood
350 (±25)	1600	1.8	(240) **250** (260)	
800 (±25)	1150	3.1	(270) **280** (290)	
925 (±25)	1025	3.4	(250) **260** (270)	
1225 (±25)	725	4.3	(270) **280** (290)	
1300 (±25)	650	4.5	(900) **930** (960)	Landslide dam failure?
1700 (±25)	ca. 200	5.8	**>35,000**	Extreme magnitude, landslide dam failure flood or lahar
1850 (±25)	ca. 200	8.7	(120) **240** (350)	Base of channel fill - magnitude overestimated?

416 *Note: single estimated dates are reported here, being derived from the age-depth model (Figure 4),
417 and may deviate slightly from modelled radiocarbon dates (BP), based on our interpretation of
418 fluvial processes that controlled the local accumulation rates at the top and base of the core.

Uncertainty margins on the reconstructed recurrence times of flood units is based on the uncertainty range of the age-depth model in the association phase of channel-fill deposition.

4.3 Flood source regions

To identify variability in sediment source regions, and potentially different triggers for flooding, we used a Principal Component Analysis (PCA) on the XRF data to compare the geochemical fingerprint of flood units (Figure 8). The main factor identified in the PCA, that explains 20.5% of the observed variations in the geochemistry, is associated with Zn, K, Ti, Rb, and Zr (Figure 8). These elements commonly co-vary with variations in grain-size, as demonstrated for the Crowley House cores and in many other studies (e.g. Jones *et al*., 2012; Wilhelm *et al*., 2018b). The second main factor, which explains ca. 16.0% of the variance, is associated with Si and Al - and negatively with Fe. Al and Fe may be associated with soil material.

Figure 8

5. Discussion

5.1 Flood activity and hydroclimate

One of the applications of palaeoflood analysis is to better understand the relationship between flooding and climate change (Benito et al. 2015; Wilhelm *et al*., 2018b). To explore this in the Whanganui we compare the record of flooding in the catchment over the last 2000 years with a range of regional and sub-hemispheric hydroclimate proxies (Figure 9). As a measure of flooding, we use the average occurrence of events that have recurrence time of more than 30 years, which is the lower threshold for flood unit sedimentation for lithofacies B at Atene. A flood activity curve identifies periods of increased and reduced flood occurrence and allows visual comparison with other hydroclimate proxy records. Periods with increased flooding in the Whanganui occurred at ca. 1450-1125, 950, 650-500, and 400-325 cal. yr BP (Figure 9h). Eden and Page (1998) reconstructed storm frequencies at Lake Tutira in the eastern North Island over the past ca. 2000 yr, and periods of increased flooding in the Whanganui match episodes of enhanced storminess at Tutira (Figure 9e). In updated work, extending the Tutira record to cover the last 7200 yr, Page *et al*. (2010) report major periods of enhanced storminess between 500-700 and 1100-1250 cal. yr BP (cf. Figure 9e), which

match closely with two periods of increased flooding in the Whanganui catchment. The peak in storminess for the period of ca. 1850 – 2100 cal. yr BP documented at Tutira (Page *et al*., 2010) is not recorded in the Whanganui because of the very significant valley floor transformations that occurred as the result of the Taupo eruption. The otherwise consistent relationship between the Whanganui flood records, river activity elsewhere in the North Island (Figure 9g), and the record of storminess from Lake Tutira (Figure 9e) suggests these are reliable records and all responding to similar climate drivers at this scale. The correlation between the higher resolution lake record at Tutira with ENSO (Page *et al*., 2010), suggests ENSO may have been the principal control of the frequency of major floods in the Whanganui catchment during the past 2000 years.

Figure 9

Looking farther afield, comparison with pan-Pacific records in South America shows some correspondence between reduced flood activity in the Whanganui with warm, dry episodes named Cipreses cycles (CC) (Moreno *et al*., 2018, Moreno *et al*., 2014) (Figure 9d). These episodes are interpreted to reflect changes in intensity and position of the Southern Hemisphere Westerly Winds (SHWW), where weakening of intensity and / or poleward shift (south) of the wind belt reduces storm frequency and intensity, resulting in warmer, drier conditions at centennial scales. Moreno *et al*. (2014) have related a wetter phase between AD 1890 and ca. AD 1300 as being contemporaneous with strongly negative anomalies in SAM inferred from tree ring data in Patagonia. The onset of this period at ca. AD 1350 coincides with a distinct period of increased flood activity in the Whanganui, which is not, however, as long-lived as the Patagonia wet-phase. Lorrey *et al*. (2014) have argued that during the New Zealand Little Ice Age (AD ~1450-1850) the generally cooler, wetter climate of this time was produced by a *combination* of weak El Niño and negative SAM conditions in the region, which is consistent with observations in Patagonia and flood activity in the Whanganui. The pan-Pacific record that perhaps shows most consistency with phases in Whanganui flood activity is the record of El Niño events from the Galapagos (Conroy *et al*., 2008) (Figure 9c). This shows periods of increased flooding in the Whanganui during La Niña-dominated phases, as was also found in the Lake Tutira record (Page *et al*., 2010). Subtropical storms and ex-tropical cyclones, and / or more slow-moving low pressure systems associated with blocking synoptic conditions (cf. Kidson 2000; Griffiths 2011), which occur more frequently during La Niña events, appear to be important flood generators in the Whanganui over multi-centennial and longer time periods. The Whanganui catchment, situated mid- and west-North Island is likely to be subject to

both westerly storms during enhanced SHWW periods, El Niño events, negative SAM (cf. Li and McGregor, 2017) *and* subtropical cyclones during La Niña events and positive SAM.

5.2 Flood source regions

In addition to floods resulting from major storms, it is feasible that large floods in the Whanganui catchment could also be generated by breaching of landslide dams emplaced as a consequence of deep-seated landslides in the narrow valley, potentially triggered by seismic activity. Large, deep-seated landslides within the catchment were certainly reported in 1838 and 1843 following large (M_w 6-7 and M_w 7.5 respectively) earthquakes (Crozier and Pillans, 1991) and anecdotal evidence has reported blockage of the river by a large landslide around this time (Watson, personal communication 2017). Furthermore, based on relative dating of landslides in the region, Crozier *et al.* (1995) postulated the existence of a large landslide-producing event around 1300 yr BP, which appears to coincide with the second largest single flood recorded in the Atene record (Table 2). Figure 10 shows an example of landslide debris (presently undated) that blocked the Whanganui valley c. 3 km downstream of Atene. Lahars from Mt. Ruapehu may also be routed into the upper catchment, although these are likely to be attenuated by the time they reach the lower reaches of the Whanganui catchment. No large-scale lahar or volcanic mass flow has been routed down the Whanganui from Ruapehu or the Volcanic Plateau as a whole since the Taupo event of AD 232 (Tost and Cronin, 2016).

Figure 10

Based on the results of the PCA (Figure 8), the overall similarity in geochemistry of flood units suggests that no discrete (sub)catchment sources can be identified for most flood events. Nonetheless, the largest flood of the Whanganui palaeoflood record appears anomalous. The event is unique in terms of its coarseness (based on the Zr/Rb ratio), but also has extremely high levels of S, Y, P, Cu, and Ca (Figure 8). These elements are located on the opposite side of the PCA spectrum from those elements that are used as grain-size indicators. The event dated to ca. AD 200 (±25) occurred just before the Taupo Eruption and its geochemical composition (e.g. depletion of K) indicates that these sediments are not of direct volcanic origin, which might rule out a lahar origin. Our preliminary interpretation of this unusual flood is that one or more landslides may have blocked the Whanganui gorge upstream and produced a large release-type event when the dam(s) was

(were) breached. The timing of this anomalous flood is though so close to the Taupo AD 232 event that some association with this disturbance would seem reasonable. A scenario is envisaged whereby the seismic shaking of the region by the Taupo eruption potentially triggered (multiple) landslide dams, which subsequently breached. This may then have been followed by plugging of the Atene meander cutoff by rafts of pumice as volcanogenic material was reworked down the river system as the valley floor was reset by the injection of this Taupo alluvium (cf. Manville *et al*., 2009). More work is required to resolve this chain of events and test this preliminary interpretation.

5.3 Comparison with Manawatu and flood risk assessments

The Whanganui flood series represents a significant advance in palaeoflood analysis in New Zealand by reconstructing for the first time an event-scale flood record over the last 2000 years and relating flood occurrence to regional climate variability. There is however a striking difference between our recent findings in the nearby Manawatu catchment (Fuller *et al*. 2018) and the Whanganui flood record in terms of the frequency of large flood events. The largest flood event in the Manawatu was observed in AD 1857 and grain-size analysis from multiple palaeochannel sites suggested this was the largest flood in the ca. 3000-year record (Fuller *et al.*, 2018). The Whanganui palaeoflood record shows conversely that prior to the 19th century there were many events which exceeded both observed and gauged floods in the catchment that have occurred since 1858. One very important implication of this new evidence for flood risk assessment in the Whanganui catchment is that reliance solely on gauged records will inevitably underestimate both the magnitude and frequency of damaging large floods such as the June 2015 event. Furthermore, with evidence that some of the largest storm-driven floods in the Whanganui River are associated with La Niña-type climate phases, warming of the adjacent Tasman Sea and western Pacific Ocean are likely to increase storm intensity from this sector of the Pacific. Finally, the recognition that probably the largest flood in the Whanganui during the last 2000 years was generated by the probable failure of landslide dam that blocked the Whanganui gorge ca. AD 200, poses a real problem for flood risk management as the occurrence and impact of these types of events are notoriously difficult to predict.

6. Conclusion

Flooding in the Whanganui catchment over the last 2000 years have been reconstructed from a unique valley meander cutoff at Atene, covering a period of time just prior to the transformation of the valley floor by the ca. AD 232 Taupo eruption. This is the first multi-millennial, event-scale record of river flooding in New Zealand and most importantly demonstrates the occurrence of several very

large flood events prior to the 19th century that exceed the magnitude of floods gauged or observed to date. It is likely that the largest of these floods was caused by breaching of a landslide dam around AD 200 that temporarily blocked the Whanganui gorge. ENSO variability (modulated by SAM) appears to be the principal climatic driver of floods in the Whanganui catchment during the last ~2000 years with multi-centennial length episodes of increased flooding associated with La Niña-type climate phases. In the context of predicted climate change, with intensification of the hydrological cycle and storm activity, it is very likely that future floods in the Whanganui River will exceed the magnitude of floods recorded and observed to date. This conclusion has important implications for catchment and hazard managers , who also need to be aware that large and damaging floods in the Whanganui, and elsewhere in New Zealand, are controlled by a complex range of factors, including hydroclimate variability, seismic-generated landslides, and land use.

Acknowledgements

We are very grateful for field assistance provided by David Feek and Erica Malloy. Funding was provided by Massey University Research Funding to ICF. We thank the Crowley family for access to their paddocks at Crowley House and Glenn Ranginui for arranging site access at Atene. We appreciate the time taken by the reviewers tasked with reading and recommending improvements to this manuscript. We also thank the Editors of this Special Issue for their invitation to contribute this work.

References

Abram, N. J., Mulvaney, R., Vimeux, F., Phipps, S. J., Turner, J. & England, M. H. 2014. Evolution of the Southern Annular Mode during the past millennium. *Nature Climate Change*, 4**,** 564.

Beatson, K.E. & Whelan, H. (1993). T*he River Flows on: Ngatimoti Through Flood and Fortune*. K. Beatson & H. Whelan.

Bard, E., Raisbeck, G., Yiou, F. & Jouzel, J. 2000. Solar irradiance during the last 1200 years based on cosmogenic nuclides. *Tellus B*, 52**,** 985-992. Available: DOI doi:10.1034/j.1600-0889.2000.d01-7.x.

Benito, G., Macklin, M.G., Panin, A., Rossato, S., Fontana, A., Jones, A.F., Machado, M.J., Matlakhova, E., Mozzi, P. & Zielhofer, C. 2015. Recurring flood distribution patterns related to short-term Holocene climatic variability. *Scientific Reports*, 5, p.16398.

Blackwood, P. & Bell, J. 2016. *Lower Whanganui River Flood Protection Investigations: Review of the June 2015 Flood and Update of Design Flood Level Estimates*. Report No: 2016/EXT/1482, Horizons Regional Council, Palmerston North, 83 pp.

582 Blöschl, G., Hall, J., Parajka, J., Perdigão, R. A., Merz, B., Arheimer, B., Aronica, G. T., Bilibashi, A.,
583 Bonacci, O. & Borga, M. 2017. Changing climate shifts timing of European floods. *Science*,
584 357**,** 588-590.

585 Braganza, K., Gergis, J. L., Power, S. B., Risbey, J. S. & Fowler, A. M. 2009. A multiproxy index of the El
586 Niño–Southern Oscillation, AD 1525–1982. *Journal of Geophysical Research: Atmospheres*,
587 114.

588 Bronk Ramsey, C. 2009. Bayesian Analysis of Radiocarbon Dates. *Radiocarbon*, 51, 337-360.

589 Crozier, M.J. & Pillans, B.J. 1991. Geomorphic events and landform response in south-eastern
590 Taranaki, New Zealand. *Catena*, 18, 471-487.

591 Crozier, M.J., Deimel, M.S. & Simon, J.S. 1995. Investigation of earthquake triggering for deep-seated
592 landslides, Taranaki, New Zealand. *Quaternary International*, 23, 65-73.

593 Conroy, J. L., Overpeck, J. T., Cole, J. E., Shanahan, T. M. & Steinitz-Kannan, M. 2008. Holocene
594 changes in eastern tropical Pacific climate inferred from a Galápagos lake sediment record.
595 *Quaternary Science Reviews*, 27**,** 1166-1180.

596 Dellow, G.D., McSaveney, M.J., Stirling, M.W., & Berryman, K.R. 2005. A probabilistic landslide
597 hazard model for New Zealand. In: J.R. Pettinga & A.M. Wandres (Eds.), GSNZ 50th Annual
598 Conference, 28 Nov. to 1 Dec. 2005, Kaikoura: Programs and Abstracts, 119A. *Geological*
599 *Society of New Zealand Miscellaneous Publication*, p. 24.

600 Dettinger, M. 2011. Climate Change, Atmospheric Rivers, and Floods in California – A Multimodel
601 Analysis of Storm Frequency and Magnitude Changes1. *JAWRA Journal of the American*
602 *Water Resources Association*, 47**,** 514-523. Available: DOI doi:10.1111/j.1752-
603 1688.2011.00546.x.

604 Eden, D.N. & Page, M.J. 1998. Palaeocclimatic implications of a storm erosion record from late
605 Holocene lake sediments, North Island, New Zealand. *Palaeogeography*, *Palaeoclimatology*,
606 *Palaeoecology*, 139, 37-58.

607 Eiby G.A. 1968. A descriptive catalogue of New Zealand earthquakes. *New Zealand Journal of*
608 *Geology and Geophysics*, 11, 30–32.

609 Ely, L. L., Enzel, Y., Baker, V. R. & Cayan, D. R. 1993. A 5000-Year Record of Extreme Floods and
610 Climate Change in the Southwestern United States. *Science*, 262**,** 410-412. Available: DOI
611 10.1126/science.262.5132.410.

612 Foulds, S. A. & Macklin, M. G. 2016. A hydrogeomorphic assessment of twenty-first century floods in
613 the UK. *Earth Surface Processes and Landforms*, 41**,** 256-270. Available: DOI
614 doi:10.1002/esp.3853.

615 Fuller, I. C., Macklin, M. G. & Richardson, J. M. 2015. The Geography of the Anthropocene in N ew Z
616 ealand: Differential River Catchment Response to Human Impact. *Geographical Research*,
617 53**,** 255-269.

618 Fuller, I. C., Macklin, M. G., Toonen, W. H. J. & Holt, K. A. 2018. Storm-generated Holocene and
619 historical floods in the Manawatu River, New Zealand. *Geomorphology*, 310**,** 102-124.
620 Available: DOI https://doi.org/10.1016/j.geomorph.2018.03.010.

621 Gallant, A.J., Phipps, S.J., Karoly, D.J., Mullan, A.B. and Lorrey, A.M., 2013. Nonstationary
622 Australasian teleconnections and implications for paleoclimate reconstructions. *Journal of*
623 *Climate*, 26, 8827-8849.

624 Gomez, B., Carter, L., Orpin, A.R., Cobb, K.M., Page, M.J., Trustrum, N.A. and Palmer, A.S. 2012.
625 ENSO/SAM interactions during the middle and late Holocene. *The Holocene*, 22, 23-30.

626 Gomez, B., Carter, L., Trustrum, N. A., Page, M. J. & Orpin, A. R. 2013. Coherent rainfall response to
627 middle- and late-Holocene climate variability across the mid-latitude South Pacific. *The*
628 *Holocene*, 23**,** 1002-1007. Available: DOI 10.1177/0959683613479679.

629 Graly, J.A., Bierman, P.R., Reusser, L.J., Pavich, M.J., 2010. Meteoric 10Be in soil profiles: a
630 global meta-analysis. *Geochimica Et Cosmochimica Acta* 74, 6814–6829.

631 Griffiths, G. 2011. Drivers of extreme daily rainfalls in New Zealand. *Weather and Climate*, 31, 24-49.

632 Heikkilä, U. 2007. *Modeling of the atmospheric transport of the cosmogenic*
633 *radionuclides ^{10}Be and ^{7}Be using the ECHAM5-HAM General Circulation Model*.
634 Ph.D. thesis. ETH-Zurich. 148 pp

635 Hicks, D. M., Shankar, U., Mckerchar, A. I., Basher, L., Lynn, I., Page, M. & Jessen, M. 2011.
636 Suspended sediment yields from New Zealand rivers. *Journal of Hydrology (New Zealand)***,**
637 81-142.

638 Hirabayashi, Y., Mahendran, R., Koirala, S., Konoshima, L., Yamazaki, D., Watanabe, S., Kim, H. &
639 Kanae, S. 2013. Global flood risk under climate change. *Nature Climate Change*, 3**,** 816.

640 Hogg, A., Lowe, D. J., Palmer, J., Boswijk, G. & Ramsey, C. B. 2012. Revised calendar date for the
641 Taupo eruption derived by ^{14}C wiggle-matching using a New Zealand kauri ^{14}C calibration
642 data set. *The Holocene*, 22**,** 439-449. Available: DOI 10.1177/0959683611425551.

643 Hogg, A.G., Hua, Q., Blackwell, P.G., Niu, M., Buck, C.E., Guilderson, T.P., Heaton, T.J., Palmer, J.G.,
644 Reimer, P.J., Reimer, R.W. and Turney, C.S. 2013. SHCal13 Southern Hemisphere calibration,
645 0–50,000 years cal BP. *Radiocarbon*, 55, 1889-1903.

646 Jiang, N., Griffiths, G. & Lorrey, A. 2013. Influence of large-scale climate modes on daily synoptic
647 weather types over New Zealand. *International Journal of Climatology*, 33, 499-519.

648 Jones, A. F., Macklin, M. G. & Brewer, P. A. 2012. A geochemical record of flooding on the upper
649 River Severn, UK, during the last 3750 years. *Geomorphology*, 179**,** 89-105. Available: DOI
650 https://doi.org/10.1016/j.geomorph.2012.08.003.

651 Kettner, A. J., Gomez, B. & Syvitski, J. P. M. 2007. Modeling suspended sediment discharge from the
652 Waipaoa River system, New Zealand: The last 3000 years. *Water Resources Research*, 43.
653 Available: DOI doi:10.1029/2006WR005570.

654 Kidson, J. W. 2000. An analysis of New Zealand synoptic types and their use in defining weather
655 regimes. *International journal of climatology*, 20**,** 299-316.

656 Kiem, A. S., Franks, S. W. & Kuczera, G. 2003. Multi-decadal variability of flood risk. *Geophysical*
657 *Research Letters*, 30. Available: DOI doi:10.1029/2002GL015992.

658 Knox, J. C. 2000. Sensitivity of modern and Holocene floods to climate change. *Quaternary Science*
659 *Reviews*, 19**,** 439-457.

660 Kundzewicz, Z. W., Kanae, S., Seneviratne, S. I., Handmer, J., Nicholls, N., Peduzzi, P., Mechler, R.,
661 Bouwer, L. M., Arnell, N., Mach, K., Muir-Wood, R., Brakenridge, G. R., Kron, W., Benito, G.,
662 Honda, Y., Takahashi, K. & Sherstyukov, B. 2014. Flood risk and climate change: global and
663 regional perspectives. *Hydrological Sciences Journal*, 59**,** 1-28. Available: DOI
664 10.1080/02626667.2013.857411.

665 Li, N. & McGregor, G.R. 2017. Linking interannual river flow river variability across New Zealand to
666 the Southern Annular Mode, 1979–2011. *Hydrological Processes*, 31, 2261-2276.

667 Longfield, S. A., Faulkner, D., Kjeldsen, T. R., Macklin, M. G., Jones, A. F., Foulds, S. A., Brewer, P. A. &
668 Griffiths, H. M. 2018. Incorporating sedimentological data in UK flood frequency estimation.
669 *Journal of Flood Risk Management***,** e12449.

Lorrey, A., Fauchereau, N., Stanton, C., Chappell, P., Phipps, S., Mackintosh, A., Renwick, J., Goodwin, I. and Fowler, A., 2014. The Little Ice Age climate of New Zealand reconstructed from Southern Alps cirque glaciers: a synoptic type approach. *Climate Dynamics*, 42, 3039-3060.

McColl, S.T. & McCabe, M. 2016. The causes and agricultural impacts of large translational landslides: Case-studies from North Island, New Zealand. In: *Landslides and Engineered Slopes. Experience, Theory and Practice*, pp. 1401-1408. CRC Press.

Macklin, M. G., & Rumsby, B. T. 2007. Changing climate and extreme floods in the British uplands. *Transactions of the Institute of British Geographers*, 32, 168-186.

Macklin, M.G., Fuller, I.C., Jones, A.F. and Bebbington, M. 2012. New Zealand and UK Holocene flooding demonstrates interhemispheric climate asynchrony. *Geology*, 40, 775-778.Manville, V., Segschneider, B., Newton, E., White, J., Houghton, B. & Wilson, C. 2009. Environmental impact of the 1.8 ka Taupo eruption, New Zealand: Landscape responses to a large-scale explosive rhyolite eruption. *Sedimentary Geology*, 220**,** 318-336.

Massey, C.I., Petley, D.N. & McSaveney, M.J. 2013. Patterns of movement in reactivated landslides. *Engineering Geology*, 159, 1-19.

Masson-Delmotte, V., Stenni, B. & Jouzel, J. 2004. Common millennial-scale variability of Antarctic and Southern Ocean temperatures during the past 5000 years reconstructed from the EPICA Dome C ice core. *The Holocene*, 14**,** 145-151. Available: DOI 10.1191/0959683604hl697ft.

Mckerchar, A. & Henderson, R. 2003. Shifts in flood and low-flow regimes in New Zealand due to interdecadal climate variations. *Hydrological Sciences Journal*, 48**,** 637-654.

Met Office Hadley Centre for Climate Change, 2016. Interdecadal Pacific Oscillation time series. Retrieved from http://cola.gmu.edu/c20c/.

Moreno, P., Vilanova, I., Villa-Martínez, R., Dunbar, R., Mucciarone, D., Kaplan, M., Garreaud, R., Rojas, M., Moy, C. & De Pol-Holz, R. 2018. Onset and evolution of southern annular mode-like changes at centennial timescale. *Scientific reports*, 8**,** 3458.

Moreno, P. I., Vilanova, I., Villa-Martínez, R., Garreaud, R. D., Rojas, M. & De Pol-Holz, R. 2014. Southern Annular Mode-like changes in southwestern Patagonia at centennial timescales over the last three millennia. *Nature Communications*, 5**,** 4375. Available: DOI 10.1038/ncomms5375 https://www.nature.com/articles/ncomms5375#supplementary-information.

Munoz, S. E. & Dee, S. G. 2017. El Niño increases the risk of lower Mississippi River flooding. *Scientific reports*, 7**,** 1772.

Munoz, S.E., Giosan, L., Therell, M.D., Remo, J.W.F., Shen, Z., Sullivan, R.M., Wiman, C., O'Donnell, M., Donnelly, J.P., 2018. Climatic control of Mississippi River flood hazard amplified by river engineering. *Nature*, 556, 95-98.

Norton, K., von Blanckenburg, F., Schlunegger, F., Schwab, M., & Kubik, P. (2008). Cosmogenic nuclide-based investigation of spatial erosion and hillslope channel coupling in the transient foreland of the Swiss Alps. *Geomorphology*, *95*(3-4), 474-486. doi:10.1016/j.geomorph.2007.07.013

Page, M., Trustrum, N., Orpin, A., Carter, L., Gomez, B., Cochran, U., Mildenhall, D., Rogers, K., Brackley, H. & Palmer, A. 2010. Storm frequency and magnitude in response to Holocene climate variability, Lake Tutira, North-Eastern New Zealand. *Marine Geology*, 270**,** 30-44.

Pillans, B. 1990. Late Quaternary marine terraces, south Taranaki- Wanganui (sheet Q22 and part sheets Q20, Q21, R21 and R22) 1:100,000. New Zealand Geological Survey Miscellaneous Series Map 18. One sheet and notes. Department of Scientific and Industrial Research, Wellington, New Zealand.

716 Qiao, Y., 2012. *Detecting signals of climatic shifts and land use change from precipitation and river*
717 *discharge variations: The Whanganui and Waikato catchments* (M.Sc. thesis, University of
718 Waikato, 215 pp, available at: https://researchcommons.waikato.ac.nz/handle/10289/6494.

719 Richardson, J., Fuller, I., Holt, K., Litchfield, N. & Macklin, M. G. 2014. Rapid post-settlement
720 floodplain accumulation in Northland, New Zealand. *Catena*, 113**,** 292-305.

721 Richardson, J., Fuller, I., Macklin, M. G., Jones, A., Holt, K., Litchfield, N. & Bebbington, M. 2013.
722 Holocene river behaviour in New Zealand: response to regional centennial-scale climate
723 forcing. *Quaternary Science Reviews*, 69**,** 8-27.

724 Schulte, L., Peña Rabadán, J. C., Ferreira De Carvalho, R. F., Schmidt, T. L., Julià Brugués, R., Llorca, J.
725 & Veit, H. 2015. A 2600-year history of floods in the Bernese Alps, Switzerland: frequencies,
726 mechanisms and climate forcing. *Hydrology and Earth System Sciences*, *2015*, *vol. 19*, *num.*
727 *7*, *p. 3047-3072*.

728 Soons, J. & Selby, M. 1992, Landforms of New Zealand. Longman Paul, Auckland.

729 Toonen, W.H., Kleinhans, M.G. and Cohen, K.M. 2012. Sedimentary architecture of abandoned
730 channel fills. *Earth Surface Processes and Landforms*, 37, 459-472.

731 Toonen, W., Winkels, T., Cohen, K., Prins, M. & Middelkoop, H. 2015. Lower Rhine historical flood
732 magnitudes of the last 450 years reproduced from grain-size measurements of flood
733 deposits using End Member Modelling. *Catena*, 130**,** 69-81.

734 Toonen, W. H. J., Middelkoop, H., Konijnendijk, T. Y. M., Macklin, M. G. & Cohen, K. M. 2016. The
735 influence of hydroclimatic variability on flood frequency in the Lower Rhine. *Earth Surface*
736 *Processes and Landforms*, 41**,** 1266-1275. Available: DOI doi:10.1002/esp.3953.

737 Toonen, W.H., Foulds, S.A., Macklin, M.G. and Lewin, J. 2017. Events, episodes, and phases: Signal
738 from noise in flood-sediment archives. *Geology*, 45, 331-334.

739 Tost, M. & Cronin, S.J. 2016. Climate influence on volcano edifice stability and fluvial landscape
740 evolution surrounding Mount Ruapehu, New Zealand. *Geomorphology*, 262, 77-90.

741 Ummenhofer, C. C. & England, M. H. 2007. Interannual extremes in New Zealand precipitation linked
742 to modes of Southern Hemisphere climate variability. *Journal of Climate*, 20**,** 5418-5440.

743 Ward, P. J., Jongman, B., Kummu, M., Dettinger, M. D., Sperna Weiland, F. C. & Winsemius, H. C.
744 2014. Strong influence of El Niño Southern Oscillation on flood risk around the world.
745 *Proceedings of the National Academy of Sciences*, 111**,** 15659-15664. Available: DOI
746 10.1073/pnas.1409822111.

747 Wilhelm, B., Arnaud, F., Sabatier, P., Crouzet, C., Brisset, E., Chaumillon, E., Disnar, J.-R., Guiter, F.,
748 Malet, E. & Reyss, J.-L. 2012. 1400 years of extreme precipitation patterns over the
749 Mediterranean French Alps and possible forcing mechanisms. *Quaternary Research*, 78**,** 1-

750 Wilhelm, B., Ballesteros Cánovas, J. A., Macdonald, N., Toonen, W. H., Baker, V., Barriendos, M.,
751 Benito, G., Brauer, A., Corella, J. P. & Denniston, R., Glaser, R., Ionita, M., Kahle, M., Liu, T.,
752 Luetscher, M., Macklin, M., Mudelsee, M., Munoz, S., Schulte, L., St. George, S., Stoffel, M. &
753 Wetter, O. 2018a. Interpreting historical, botanical, and geological evidence to aid
754 preparations for future floods. *Wiley Interdisciplinary Reviews: Water***,** e1318.

755 Wilhelm, B., Ballesteros Canovas, J. A., Corella Aznar, J. P., Kämpf, L., Swierczynski, T., Stoffel, M.,
756 Støren, E. & Toonen, W. 2018b. Recent advances in paleoflood hydrology: From new
757 archives to data compilation and analysis. *Water Security*, 3**,** 1-8. Available: DOI
758 https://doi.org/10.1016/j.wasec.2018.07.001.

759 Willenbring, J.K., von Blanckenburg, F., 2010. Meteoric cosmogenic Beryllium-10
760 adsorbed to river sediment and soil: applications for Earth-surface dynamics.
761 *Earth-Science Reviews* 98, 105–122.

762 Wilmshurst, J. M., Eden, D. N. & Froggatt, P. C. 1999. Late Holocene forest disturbance in Gisborne,
763 New Zealand: a comparison of terrestrial and marine pollen records. *New Zealand Journal of*
764 *Botany*, 37**,** 523-540.

765 Wittmann, H., von Blanckenburg, F., Bouchez, J., Dannhaus, N., Naumann, R., Christl, M., Gaillardet,
766 J., 2012. The dependence of meteoric 10Be concentrations on particle size in Amazon River
767 bed sediment and the extraction of reactive 10Be/9Be ratios. *Chemical Geology*, 318-319,
768 126-138.

769 Xia, Z., Yu, Z. & Loisel, J. 2018. Centennial-scale dynamics of the Southern Hemisphere Westerly
770 Winds across the Drake Passage over the past two millennia. *Geology*, 46**,** 855-858.

771

772

773

774

775 **Figure Captions**

776 **Figure 1.** (a) Whanganui catchment location within New Zealand, shaded black; (b) hillshade DEM of
777 the Whanganui catchment, with the main stem of the Whanganui River identified showing locations
778 of sample sites, gauging site at Te Rewa, Lake Taupo, the approximate extent of ignimbrite emplaced
779 in the ca. AD 232 eruption (white dashed line) from Manville *et al*. (2009), and approximate extent of
780 Whanganui Gorge (black dashed line alongside river); (c) contemporary land cover in the catchment;
781 (d) core location at Crowley House (1 & 2) shown on a LiDAR-DEM (LiDAR supplied by Horizons
782 Regional Council): the yellow surfaces represent relatively high Taupo terrace levels, core locations
783 are marked by the dots.; (e) core location at Atene; (f) Whanganui Gorge for context; (g) annotated
784 photograph of Atene coring site; (h) annotated photograph of Crowley House coring site; (i)
785 annotated photograph of valley meander cutoff neck at Atene for context.

786 **Figure 2.** Annual peak discharge record from Te Rewa gauging station (AD 1958-2015), and
787 estimated historical flood discharges (before AD 1958) from stage information at Whanganui City.
788 Source: Horizons Regional Council, personal communication.

789 **Figure 3.** Correlation between the D_{50} of grain-size measurements and the Zr/Rb ratio; composite
790 data from both Crowley House sites.

791 **Figure 4.** Age-depth model (for individual dates see Table 1), general lithology and XRF geochemistry
792 measurements (cps = counts per second) of the Atene core.

793 **Figure 5**. Taupo Pumice Alluvium plug at end of Atene valley meander cutoff.

794 **Figure 6.** Crowley House cores; left frame Crowley House 1 (CH1), right frame Crowley House 2
795 (CH2). Main lithological trends and variations in coarseness (Zr/Rb ratio) are shown. Both cores have
796 modern Lead (Pb) contamination in the upper parts. The Zr/Rb peak in the top of CH1 is related to
797 the deposits of the 2015 flood (inset photo, lighter colouring). A depth of a single AMS radiocarbon
798 date in CH1 is indicated by the diamond (and calibrated date). Meteoric ^{10}Be concentration and
799 indicative erosion rates for the Crowley House core. The erosion rates are calculated assuming a ^{10}Be
800 flux of 1.1×10^6 atoms/cm^2/yr and a sediment density of 1.2 g/cm^3 following Willenbring and von
801 Blanckenburg (2010). Interpreted zones of surface and deep erosion are based on the assumption of
802 a subsurface peak in ^{10}Be concentrations (e.g. Graly *et al*., 2010).

Figure 7. Left frame: Atene Zr/Rb ratios (left) with the moving window (n=101) that was used for detrending. Middle frame: detrended and normalised (Z-scored) grain-size information. Right frame: palaeoflood chronology (Lithofacies A and B), and storminess (Lithofacies C) with a calculated recurrence time for each event layer. The variations in the magnitude threshold for event registration is shaded in grey (i.e. no floods recorded in this domain); corresponding with the zonation in general lithology and changes in local setting.

Figure 8. Principal component analysis (PCA) of the Atene XRF data (left frame), and anomalous geochemistry of the large ca. AD 200 flood, found at c. 5.8 m core depth (shaded in grey, right frame). Elements with extremely low counts at the level of the event are in the PCA marked by square symbols, extremely high counts are marked by diamond symbols.

Figure 9. Comparison of (hydro)climatic records: (A) Total Solar Irradiance curve (Bard *et al*., 2000); (B) Southern Annular Mode (SAM) index (70-yr filtered; Abram *et al*., 2014); (C) Frequency of El-Niño events from the Galapagos Islands (Conroy *et al*., 2008); (D) Patagonian drought indices - charcoal densities (curve) and Cipreses dry phases (horizontal grey bars; Moreno *et al*., 2014); (E) Lake Tutira storminess (NE of North Island in New Zealand) index curve (Eden and Page, 1998) and phases (horizontal grey bars) of increased storm occurrence (Page *et al*., 2010); (F) Antarctica EPICA Dome C ice core temperature anomalies (Masson-Delmotte *et al*., 2004), averaged per century as an indicator for SAM strength (after Gomez *et al*., 2012); (G) Probability distribution based on 'activity' dates for fluvial environments on Northland, New Zealand (Richardson *et al*., 2014); (H) Flood activity of the Whanganui River, based on the frequency of large events (>30-yr recurrence time), averaged over a moving 150-yr window (this study). Periods of prolonged above-average Whanganui flood occurrence are shaded in grey in the background.

Figure 10. Historic landslide deposits on the valley floor near Atene (downstream), labelled undulating hummocky topography is attributed to landslide debris.

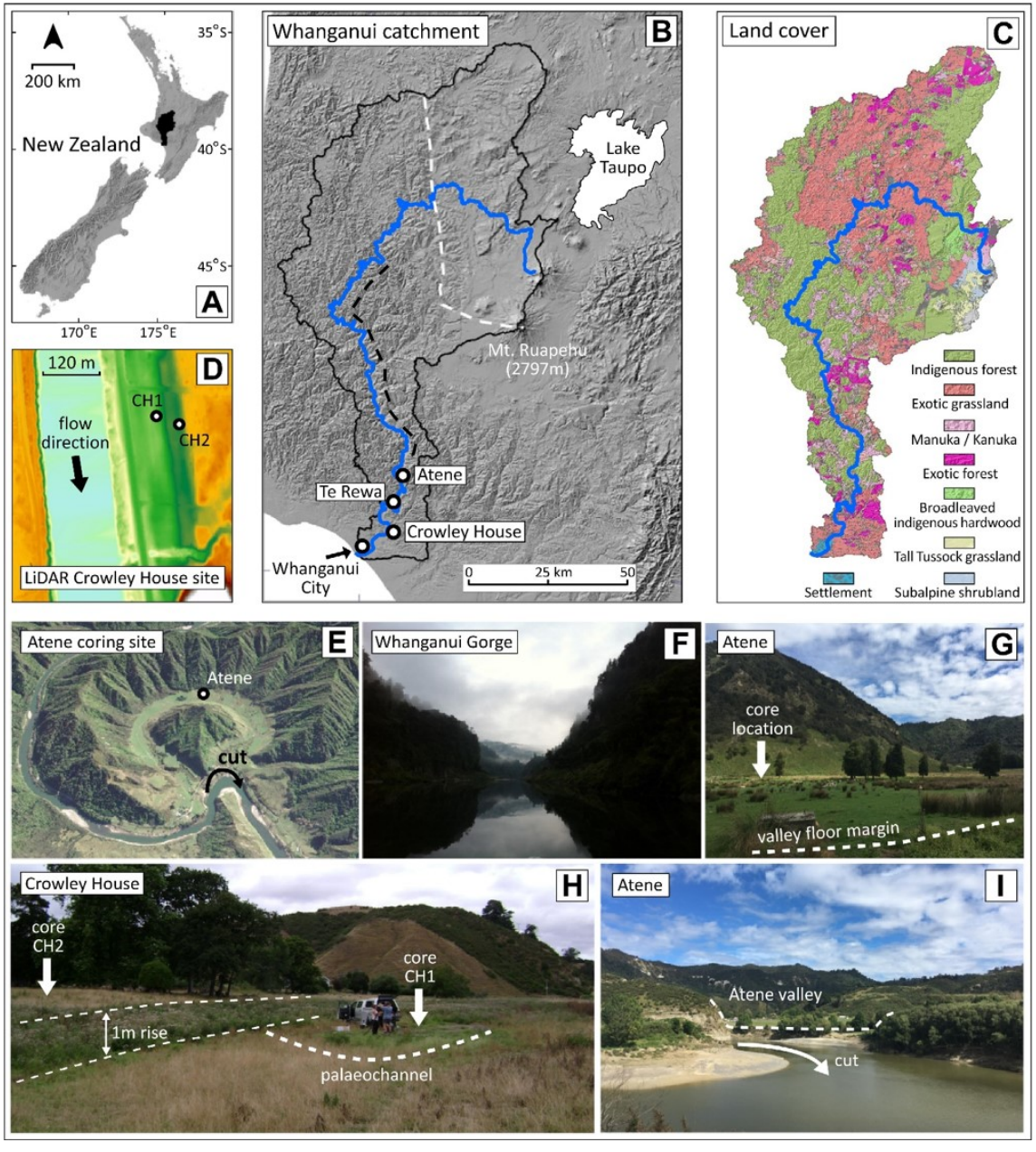
A
200 km
New Zealand
35°S
40°S
45°S
170°E
175°E
B
Whanganui catchment
Lake Taupo
Mt. Ruapehu (2797m)
Atene
Te Rewa
Crowley House
Whanganui City
0
25 km
50
C
Land cover
Indigenous forest
Exotic grassland
Manuka / Kanuka
Exotic forest
Broadleaved indigenous hardwood
Tall Tussock grassland
Settlement
Subalpine shrubland
D
120 m
CH1
CH2
flow direction
LiDAR Crowley House site
E
Atene coring site
Atene
cut
F
Whanganui Gorge
G
Atene
core location
valley floor margin
H
Crowley House
core CH2
core CH1
1m rise
palaeochannel
I
Atene
Atene valley
cut

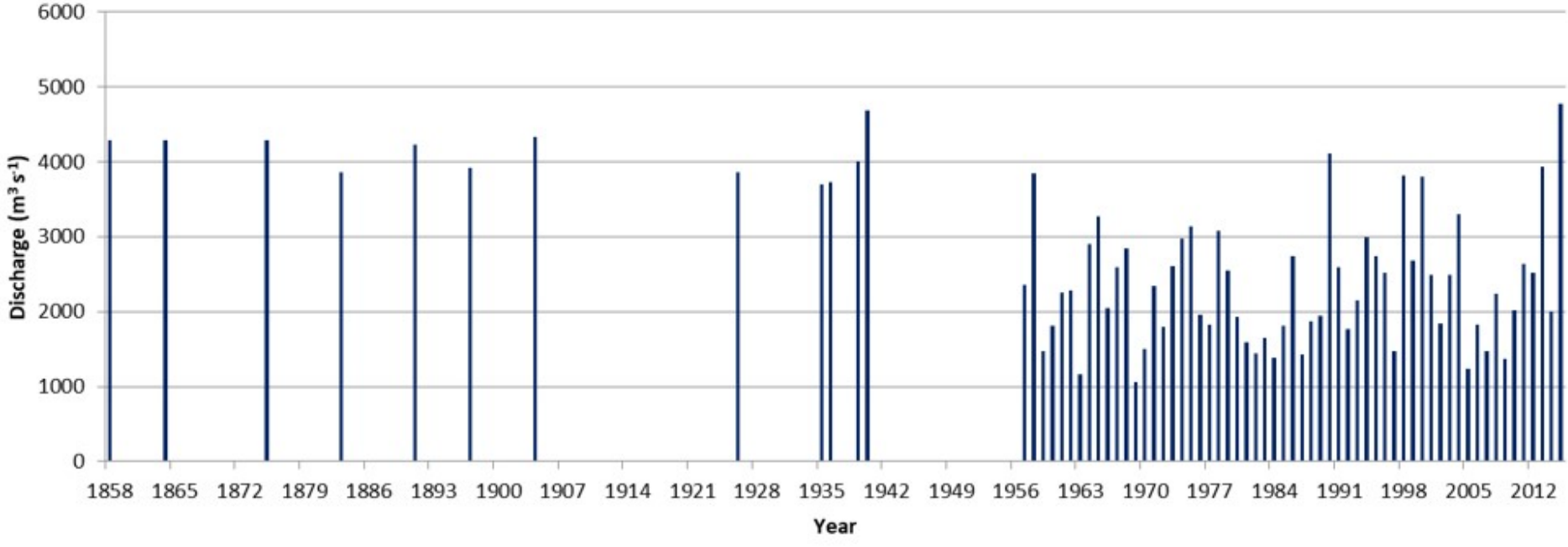
6000
5000
4000
3000
2000
1000
0
Discharge (m³ s⁻¹)
1858
1865
1872
1879
1886
1893
1900
1907
1914
1921
1928
1935
1942
1949
1956
1963
1970
1977
1984
1991
1998
2005
2012
Year

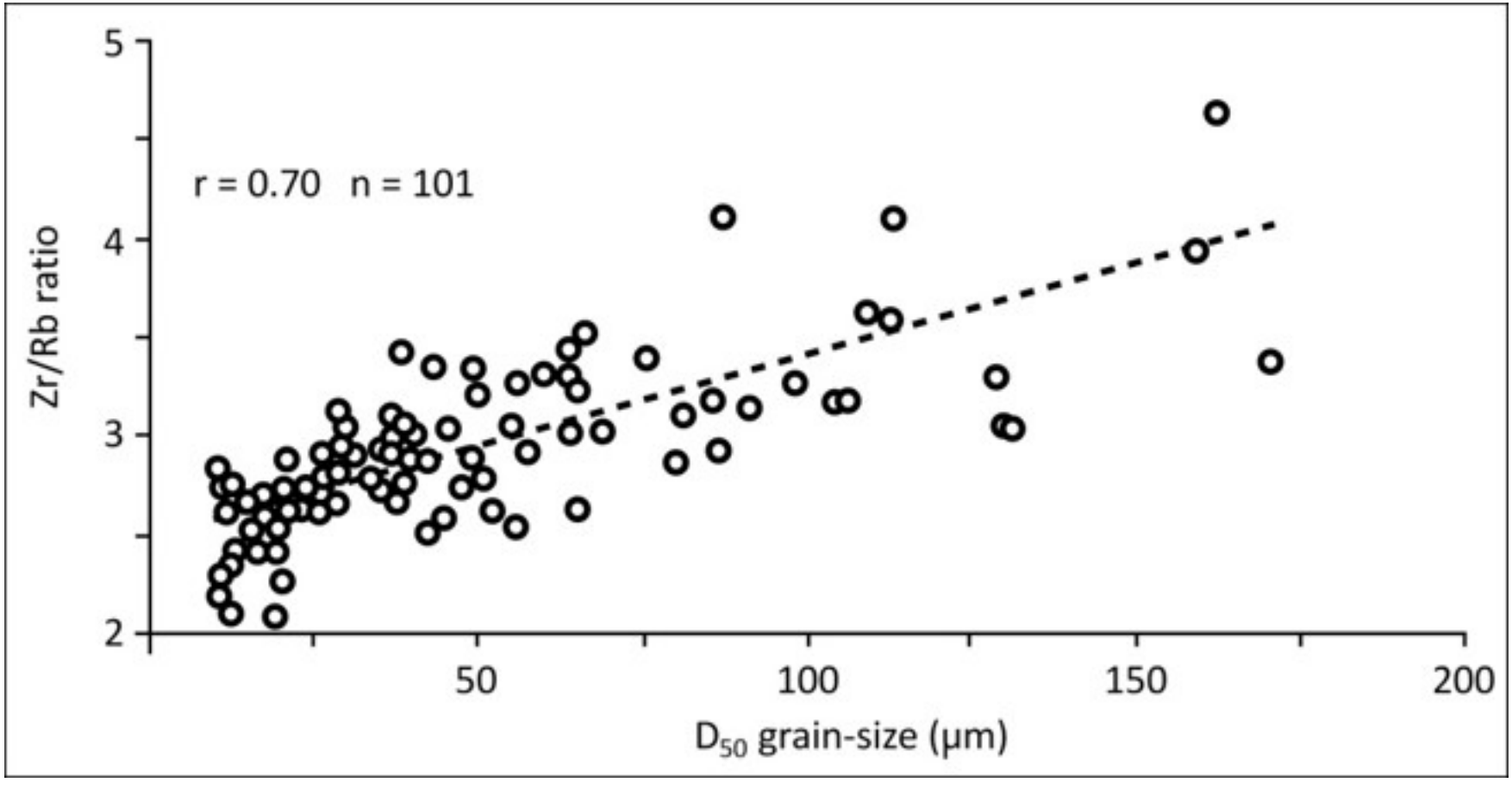
r = 0.70 n = 101
Zr/Rb ratio
5
4
3
2
50
100
150
200
D50 grain-size (µm)

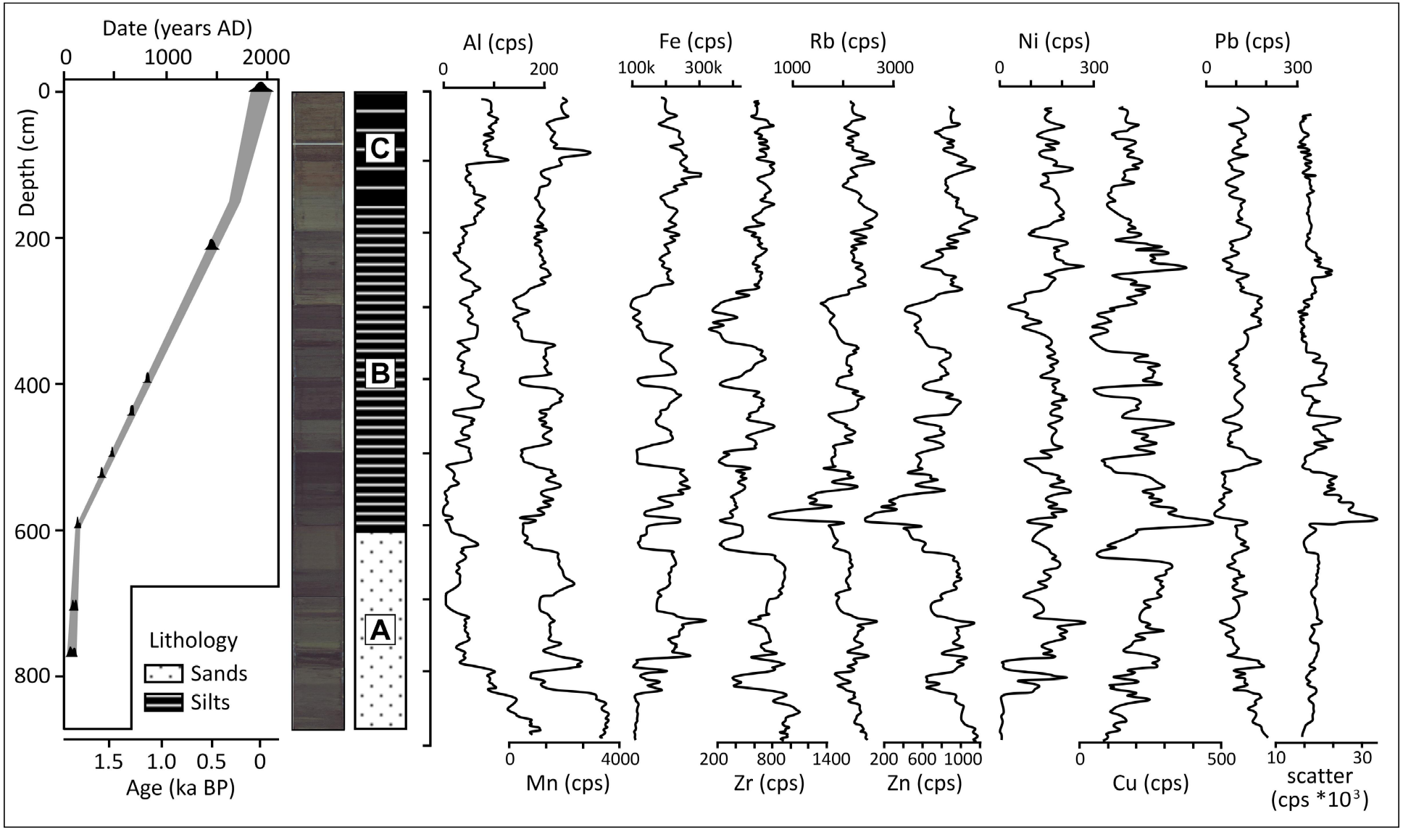
Date (years AD)
0
1000
2000
Depth (cm)
0
200
400
600
800
1.5
1.0
0.5
0
Age (ka BP)
Lithology
Sands
Silts
C
B
A
Al (cps)
0
200
Fe (cps)
100k
300k
Rb (cps)
1000
3000
Ni (cps)
0
300
Pb (cps)
0
300
0
4000
Mn (cps)
200
800
1400
Zr (cps)
200
600
1000
Zn (cps)
0
500
Cu (cps)
10
30
scatter
(cps *10³)

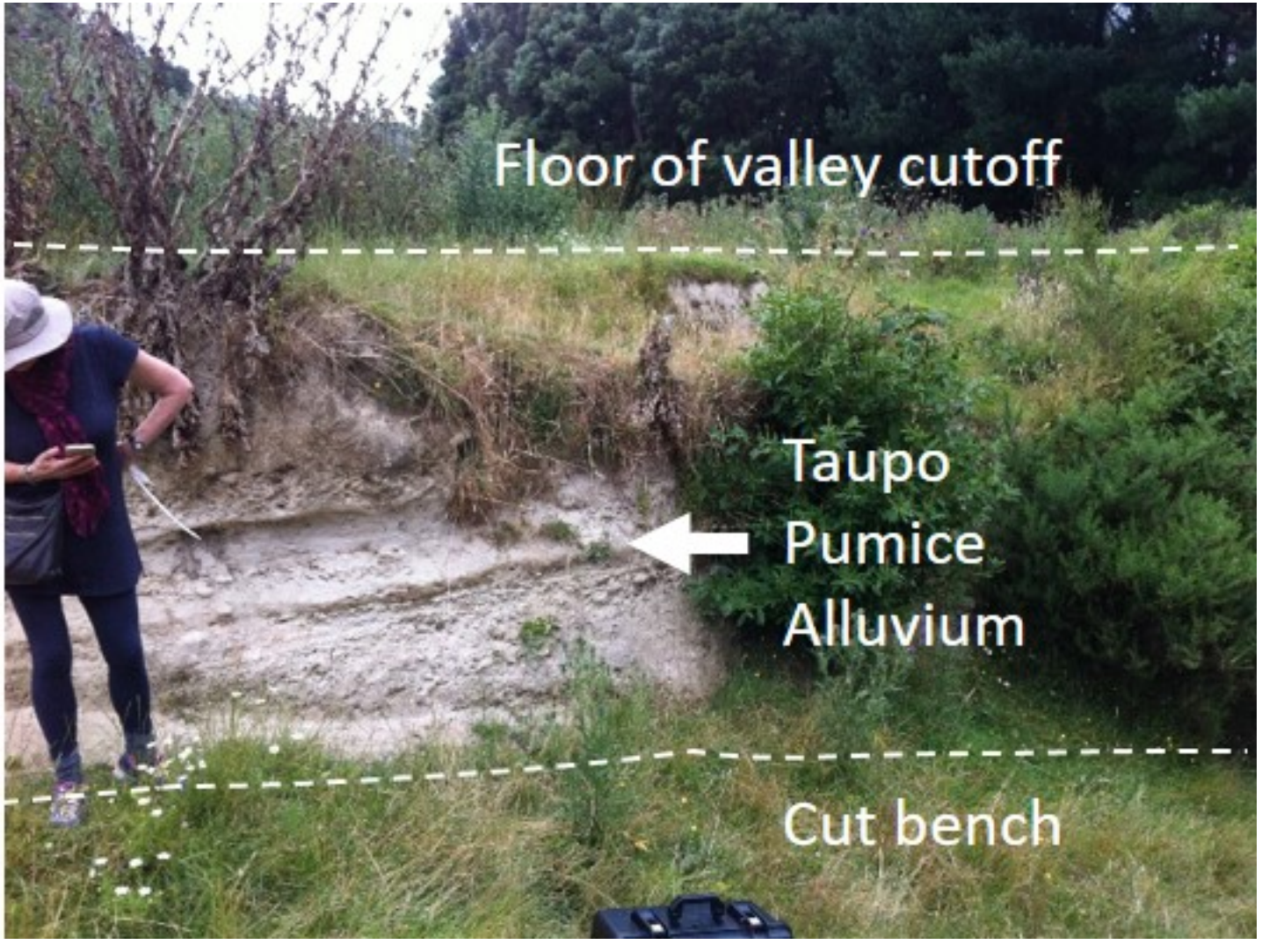
Floor of valley cutoff
Taupo
Pumice
Alluvium
Cut bench

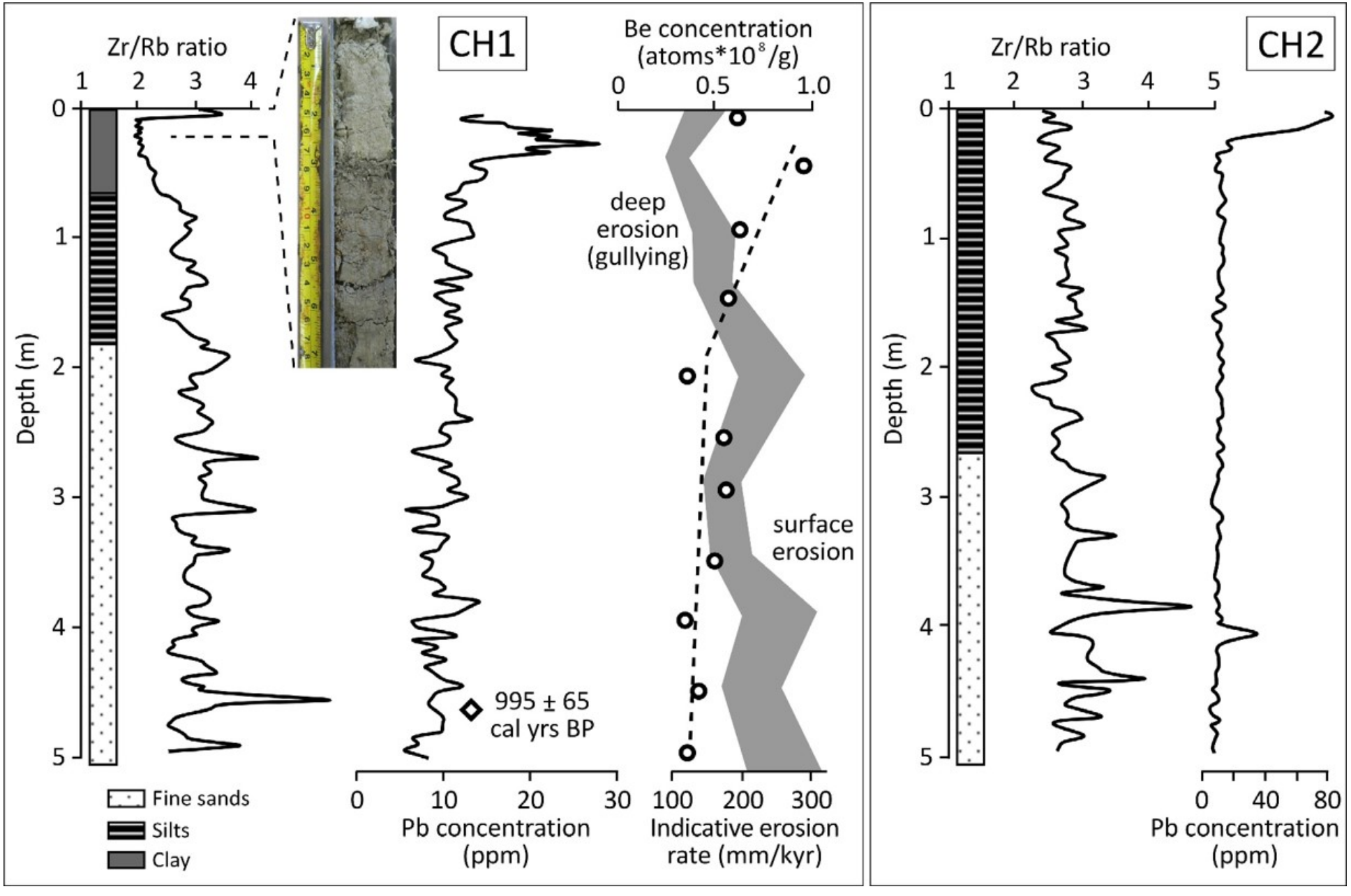
CH1
Zr/Rb ratio
1
2
3
4
0
1
2
3
4
5
Depth (m)
Be concentration
(atoms*10^{8}/g)
0
0.5
1.0
deep
erosion
(gullying)
surface
erosion
995 ± 65
cal yrs BP
0
10
20
30
Pb concentration
(ppm)
100
200
300
Indicative erosion
rate (mm/kyr)
Fine sands
Silts
Clay
CH2
Zr/Rb ratio
1
2
3
4
5
0
1
2
3
4
5
Depth (m)
0
40
80
Pb concentration
(ppm)

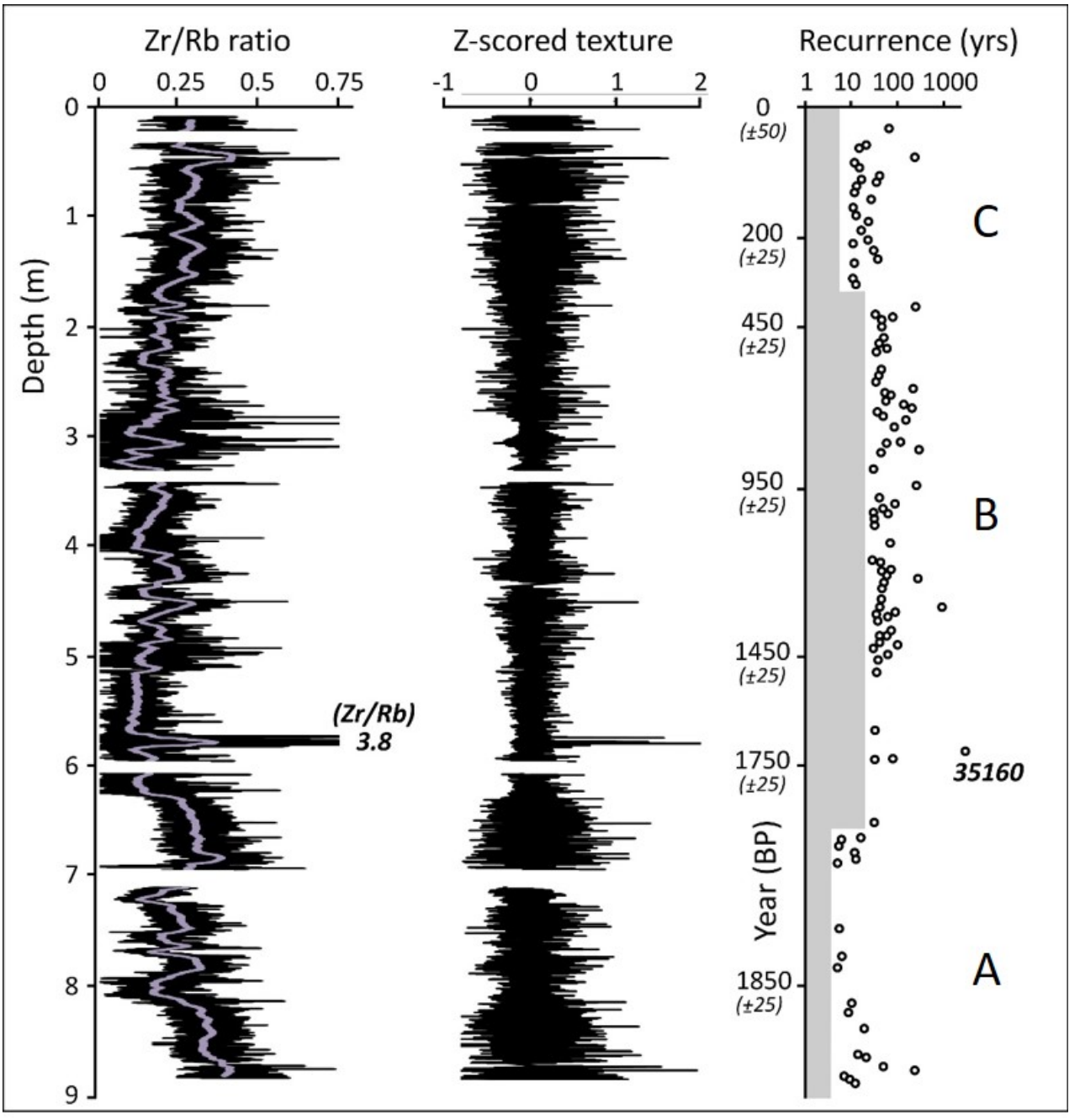
Zr/Rb ratio
0
0.25
0.5
0.75
Z-scored texture
-1
0
1
2
Recurrence (yrs)
1
10
100
1000
Depth (m)
0
1
2
3
4
5
6
7
8
9
(Zr/Rb)
3.8
0
(±50)
200
(±25)
450
(±25)
950
(±25)
1450
(±25)
1750
(±25)
1850
(±25)
Year (BP)
C
B
A
35160

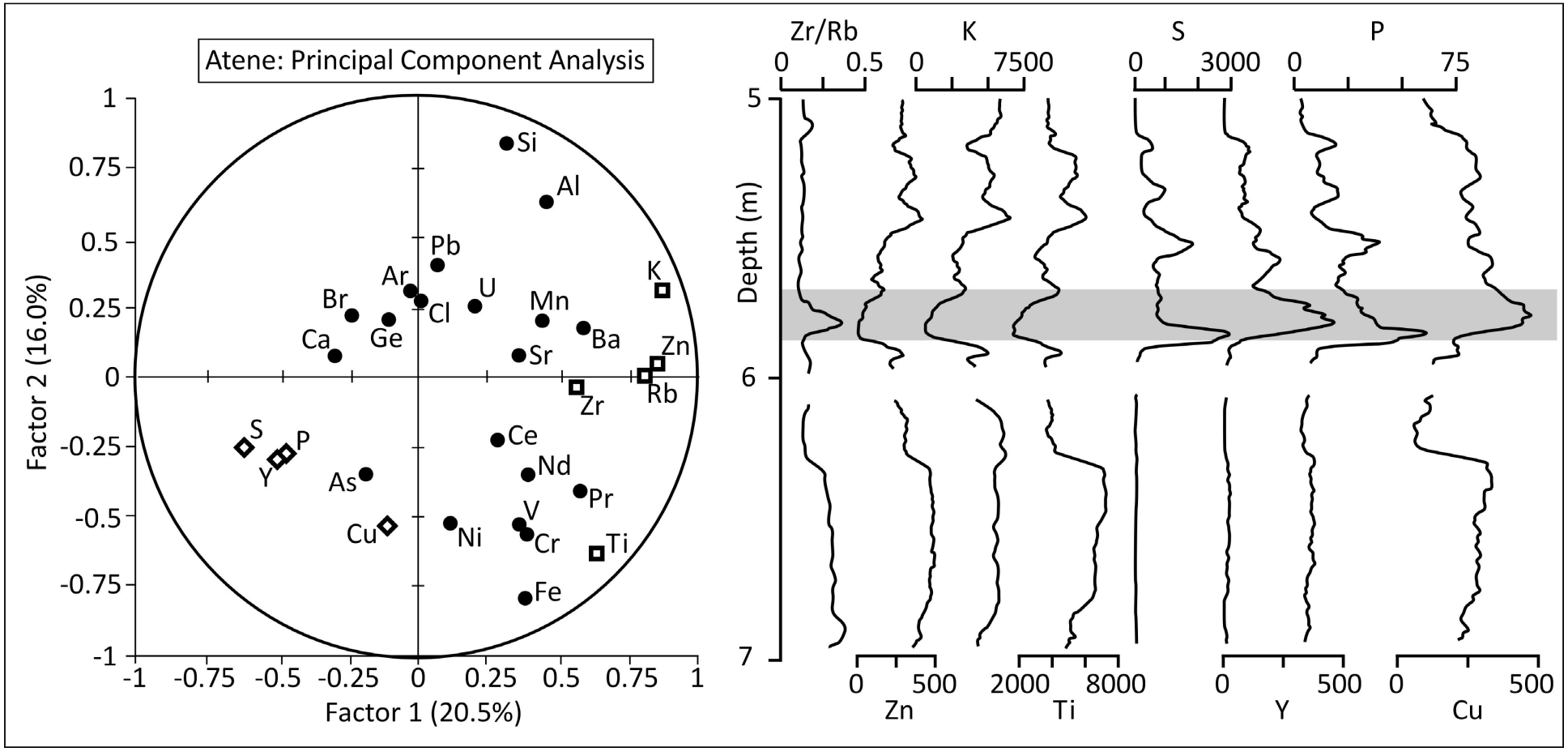
Atene: Principal Component Analysis
Factor 2 (16.0%)
Factor 1 (20.5%)
Si
Al
Pb
Ar
U
K
Br
Cl
Mn
Ca
Ge
Ba
Sr
Zn
Rb
Zr
S
P
Y
Ce
Nd
As
Pr
V
Cu
Ni
Cr
Ti
Fe
Zr/Rb
K
S
P
Depth (m)
Zn
Ti
Y
Cu

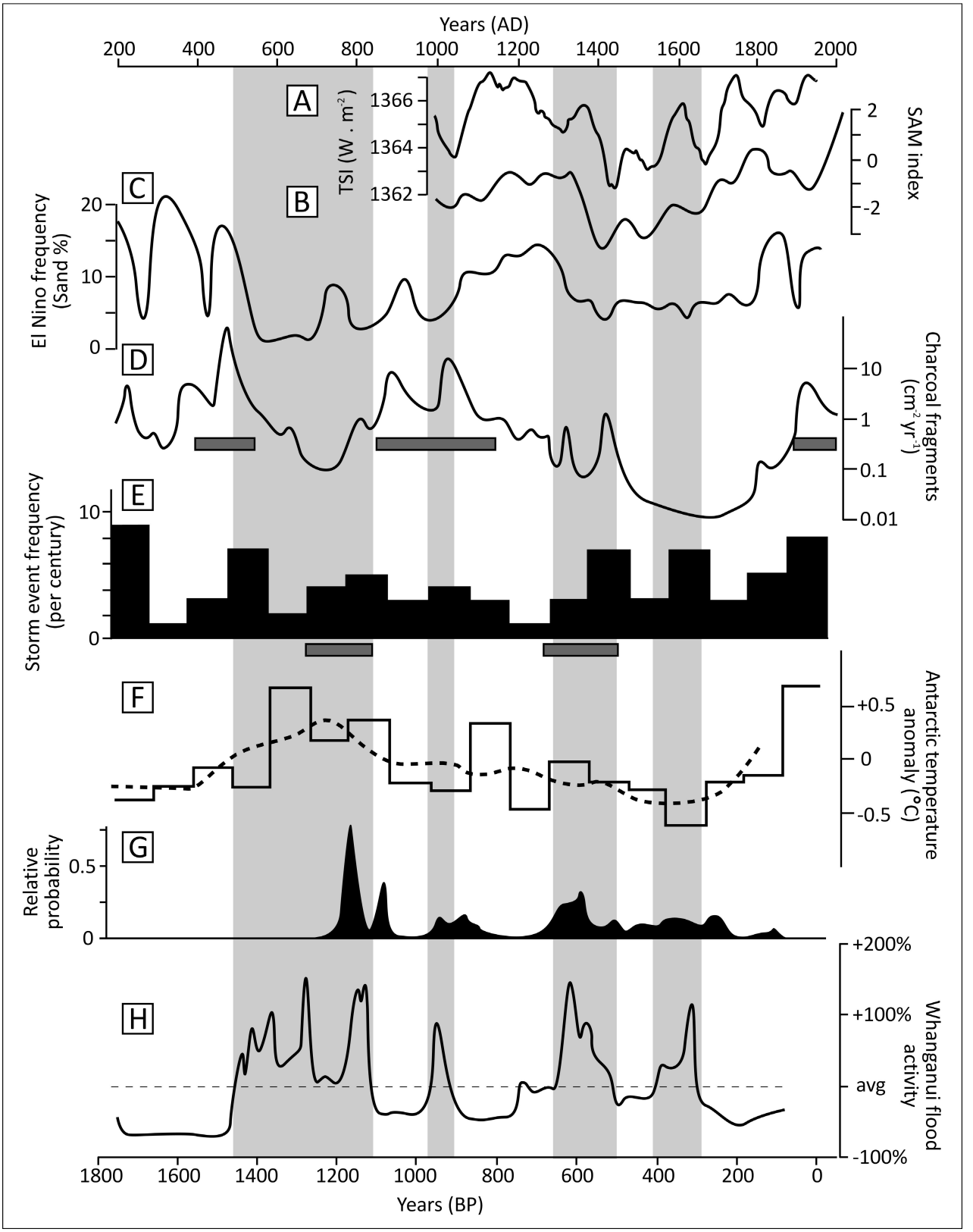
Years (AD)
200
400
600
800
1000
1200
1400
1600
1800
2000
A
TSI (W . m-2)
1366
1364
1362
B
SAM index
2
0
-2
C
El Nino frequency (Sand %)
20
10
0
D
Charcoal fragments (cm2 yr-1)
10
1
0.1
0.01
E
Storm event frequency (per century)
10
0
F
Antarctic temperature anomaly (°C)
+0.5
0
-0.5
G
Relative probability
0.5
0
H
Whanganui flood activity
+200%
+100%
avg
-100%
1800
1600
1400
1200
1000
800
600
400
200
0
Years (BP)


Landslide
hummocks